Computers and Geotechnics 138 (2021) 104361

Contents lists available at ScienceDirect

Computers and Geotechnics

journal homepage: www.elsevier.com/locate/compgeo

Mechanical behavior of frozen soils: Experimental investigation and numerical modeling

Ajay Shastri [a,b], Marcelo Sánchez [a,*], Xuerui Gai [a], Moo Y. Lee [c], Thomas Dewers [d]

[a] Zachry Department of Civil and Environmental Engineering, Texas A&M University, College Station, TX, USA
[b] Geosyntec Consultants Inc, Houston, TX, USA
[c] Geomechanics, Sandia National Laboratories, Albuquerque, NM, USA
[d] Nuclear Waste Disposal Research and Analysis, Sandia National Laboratories, Albuquerque, NM, USA

ARTICLE INFO

Keywords:
Frozen soils
Mechanical behavior
Experiments
Natural samples
Elastoplastic model
Numerical simulation
Thawing
Ground settlement

ABSTRACT

The mechanical behavior of frozen soils plays a central role in the design, construction, and maintenance of buildings and infrastructure in cold regions. We present and discuss the main results of an experimental campaign focused on the mechanical behavior of frozen soils from Alaska. The data set is unique because it involves natural frozen soils and covers a wide range of temperatures (i.e., from −6 °C up to −26 °C) and confinements (i.e., from unconfined conditions up to a cell pressure of 54.6 MPa). An elastoplastic model for frozen soils is presented and validated based on the test results. The elastoplastic model accounts for the effects of temperature and cryogenic suction on key properties associated with frozen soil behavior, namely, increase of preconsolidation pressure, stiffness, and strength with the decrease of temperature. Other aspects such as the volumetric behavior of frozen soils at different temperatures and the smooth transition between elastic and plastic states are also qualitatively well captured by the model. We implemented the constitutive model in a fully coupled thermo-hydro-mechanical simulator and we analyzed the behavior of a foundation in a thawing ground. The proposed approach is able to capture the main feature of frozen soil behavior.

1. Introduction

A substantial portion (24%) of the northern hemisphere is covered under permafrost (Andersland and Ladanyi 2003). The behavior of these soils plays a critical role in all human activities in these regions. The study of frozen soils is also important because of the recent discovery of fossil fuels, such as petroleum and gas hydrates near the Arctic Circle. The development and transport of these resources require the implementation of major engineering works. However, several problems persist in these regions, namely: distress of foundations triggered by thawing; differential movements caused in road pavements (and other civil infrastructure) due to soil heaving; glacial and periglacial slope movements; and railroad distortion. The possible effects of climate change on frozen regions have further increased the interest in this type of problem (Parry 2007). Critical engineering properties of frozen soils (e.g., strength, stiffness, and permeability) are drastically affected by the temperature.

The mechanical behavior of frozen soils has been actively investigated in the last few decades, with contributions associated with experimental investigation (both laboratory and field) and numerical modeling. Laboratory tests have allowed gaining a better understanding of the mechanical behavior of frozen soils under hydrostatic and shearing paths (e.g., Arenson et al. 2004; Chen et al. 2020; Ma and Chang 2002; De Guzman et al. 2018; Beier and Sego 2008; Parameswaran and Jones 1981; Parameswaran 1980; Sayles 1974; Wang et al. 2018; Xu et al. 2019; Yamamoto and Springman 2014; Yang et al. 2010; Chuvilin et al. 2018; Zhang et al., 2016a; 2016b; 2016c; Zhao et al. 2020; Zheng et al. 2010; Zhu et al. 2020; Da Re et al. 2003; Esmaeili-Falak et al. 2018; Esmaeili-Falak et al. 2020; Czurda and Hohmann 1997; Kim et al. 2018; Liu et al. 2020; Liu et al. 2019). The collection of frozen undisturbed samples from the field is challenging and expensive. Therefore, most of the experiments reported in the literature have been conducted on reconstituted specimens. In some works, undisturbed soil samples were retrieved in-situ (unfrozen) and were then frozen in the lab before testing them (e.g., Cui et al. 2014; Tang et al. 2018; Zhou et al. 2018). Field investigations and case studies involving freezing temperatures have also been reported in the literature (e.g., Zhukov 1990; Watson et al. 1973; Zhang et al., 2016a; 2016b;

* Corresponding author.
E-mail address: msanchez@civil.tamu.edu (M. Sánchez).

https://doi.org/10.1016/j.compgeo.2021.104361

Available online 27 July 2021

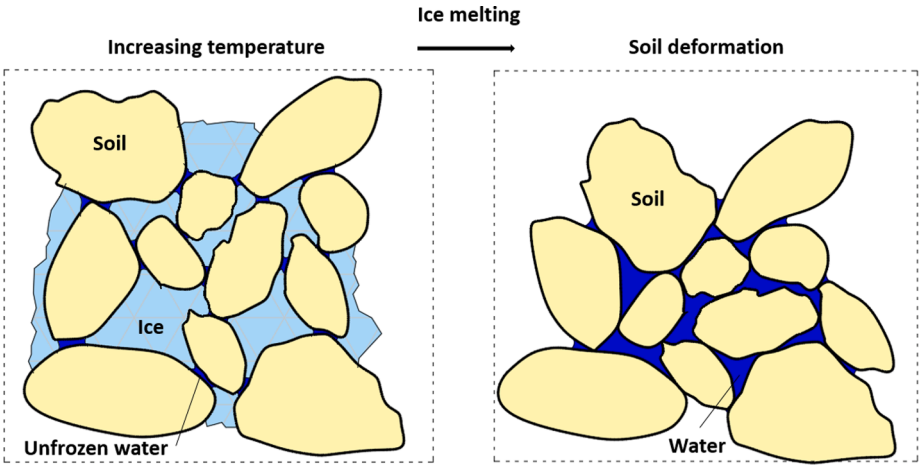

Fig. 1. Schematic representation of, a) frozen soil, and b) thawed soil (with the associated volume change).

2016c; Zhang and Michalowski 2015; Zhang et al. 2017; Goldman 2002). The focus of those works ranged from the study of geo-structure failures (e.g., Zhukov 1990; Watson et al. 1973; Goldman 2002) to actual field behavior (e.g., Zhang et al., 2016a; 2016b; 2016c; Zhang et al. 2017).

A variety of methods, approaches, and assumptions have been considered to model the behavior of frozen soils. For instance, some models are based on idealizing the frozen soil as a composite material made up of soil particles and ice (e.g., Arenson and Springman, 2005; Michalowski and Zhu 2006). Other contributions have suggested evolution laws for tracking the changes in porosity and volume during freezing (e.g., Multon et al. 2012; Nixon 1990; Kim 2011). Models to describe the progressive soil heave observed in frozen regions have also been proposed (e.g., Kim et al. 2018; Michalowski and Zhu 2006; Sheng et al. 1995; Sheng et al. 2014; Zhang et al., 2016a; 2016b; 2016c). Several approaches have been suggested to model the response of soils subjected to freeze–thaw, namely, the rigid ice model (e.g., Gilpin 1980; Miller et al., 1975; O'Neill and Miller 1985), the hydrodynamic models (e.g., Jame and Norum 1980; Harlan 1973; Newman and Wilson 1997), and the segregation potential models (e.g., Konrad and Morgenstern 1980; 1981; 1984; Konrad and Shen 1996). Shoop et al. (2008).

More recently, fully coupled thermo-hydro-mechanical (THM) formulations have been proposed to model the response of frozen soils (e.g., Zheng et al. 2010; Li et al. 2002; Thomas et al. 2009; Liu and Yu 2011; Bekele et al. 2017; Nishimura et al. 2009). The model proposed by Nishimura et al. (2009) was able to capture two key aspects related to the mechanical behavior of frozen soils, namely, soil stiffening with the decrease of temperature, and volumetric compression collapse upon thawing. The approaches proposed by Zhang and Michalowski (2015) and Zhang et al. (2016a) can also model these features of frozen soil behavior. The response of frozen soil subjected to long-term low-level repeated loading was investigated in the laboratory by Li et al. (2016a), and an associated constitutive model was proposed by Li et al. (2016b). The time-dependent behavior of frozen soils has been modeled using creep (e.g., Andersland and Ladanyi, 2003; Nixon 1990; Arenson et al. 2007) and viscoplastic models (e.g., Ghoreishian et al. 2016).

In this work, we present the main results of an experimental campaign performed at Sandia National Laboratories to study the behavior of natural frozen soil samples from Alaska at different freezing temperatures. These experiments expand the range of information involving natural frozen soils, which is almost inexistent. Furthermore, these tests cover a wide range of confinements (i.e., unconfined and triaxial tests at cell pressures up to 54.6 MPa), and freezing temperatures (i.e., from −3°C up to −26 °C). Based on these experiments, we developed and validated an elastoplastic mechanical model for frozen soils. To study the possible impact that soil thawing could have on geotechnical problems, we implemented the constitutive model in a fully coupled THM finite element program adapted for dealing with freezing temperatures. As an application case, we analyze the settlement of a building subjected to soil thawing.

In the following sections we present first some basic concepts related to frozen soil behavior. Next, we discuss the experimental campaign involving natural frozen soils from Alaska. Subsequently, we present the mechanical constitutive model and the THM framework proposed to analyze engineering problems involving frozen soils. Finally, we discuss the case study and finish with the main conclusions of this work.

2. Behavior of frozen soils

In this section we discuss the presence of unfrozen-water in frozen soils and some typical features related to the mechanical behavior of frozen soils reported in the literature.

2.1. Unfrozen water in frozen soils

Several fundamental aspects related to the effect of freezing temperature on soils have been investigated in the literature, as discussed above. Of particular interest for the research we present in this paper is the presence of unfrozen water in frozen soils, and the associated cryogenic suction (e.g., Tice et al. 1989; Williams 1964; Hohmann 1997). The pore-water does not completely freeze when the temperature reduces below the freezing point of the water (Taber 1929). The presence of unfrozen water is mainly attributed to the capillary phenomenon. Beskow (1935) observed that larger pores freeze at higher temperatures than smaller ones. Williams (1964) investigated the presence of unfrozen water in soils and its relationship with soil moisture and suction. Tice et al. (1989) confirmed the relationship between temperature and unfrozen water content. More recent works in this area have focused on the effect of pore size distribution on unfrozen water (e.g., Multon et al., 2012; Coussy 2005; Vitel et al. 2016).

Fig. 1a shows a schematic representation of a frozen soil, including the three phases, namely: liquid (unfrozen) water, frozen (ice) water, and solid (consisting of the soil mineral). The equilibrium between the ice and the unfrozen water can be expressed using the Clausius-Clapeyron equation (Clausius 1850; Clapeyron 1834), which establishes the relationship between the pressures of two phases of a single constituent material at a specified temperature, as follows:

$$P_i = \frac{\rho_i}{\rho_l} P_l - \rho_i L \ln\left(\frac{T}{273.15}\right) \quad (1)$$

where P_l [N/m^2] and P_i [N/m^2] are the unfrozen-water (in liquid state) and ice (in solid state) pressures, respectively; ρ_l and ρ_i are the water and

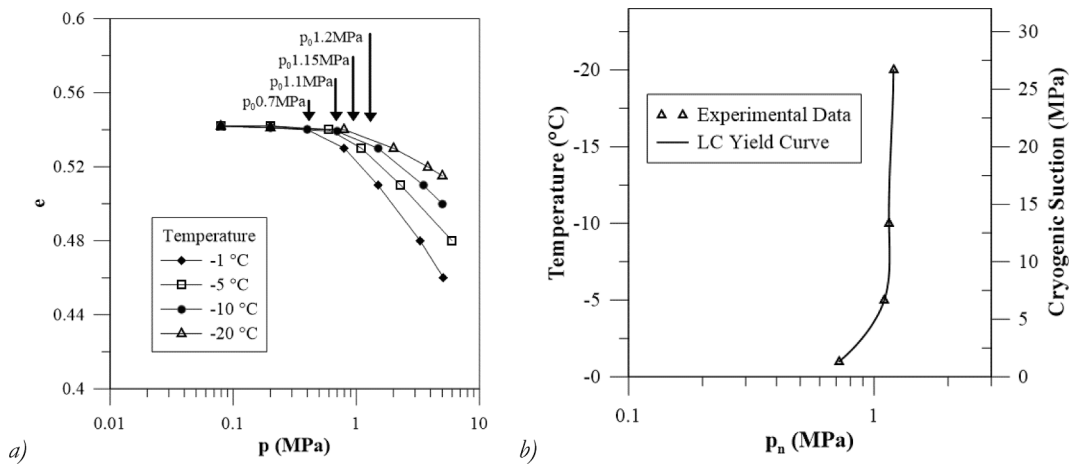

Fig. 2. Behavior of reconstituted frozen soil samples: a) isotropic behavior, Qi et al. (2010); b) variation of the preconsolidation pressure with subzero temperatures and cryogenic suction.

ice densities, respectively; L [334 kJ/kg] is the latent heat of fusion; and T [°C] is the current temperature.

The cryogenic suction (s [MPa]) can be defined as the difference between the ice and liquid pressures and it is always higher than zero:

$$s = \max(P_i - P_l, 0) \quad (2)$$

Tice et al. (1973) proposed one of the first models to account for the amount of unfrozen water in frozen soils. Tice's model relates partial saturation of liquid water (i.e., S_l [dimensionless], defined as the volume of liquid water with respect to the volume of voids) with the freezing temperature through a power law. This model involves only one constant that needs to be determined experimentally. Nishimura et al. (2009) proposed an alternative approach to predict the amount of unfrozen water in frozen soils based on the van Genuchten model (1980), typically used in unsaturated soil mechanics.

2.2. Mechanical behavior of reconstituted frozen samples

Qi et al. (2010) conducted a series of hydrostatic tests on reconstituted soils at different freezing temperatures. The samples gathered from the Qinghai-Tibet highway correspond to a low plasticity clay dried and pulverized to a size less than 2 mm. The soil was mixed with water to create a slurry compressed to create samples 100 mm diameter and 100 mm height. These samples were frozen up to −35 °C for 3 h and then maintained at the target testing temperature for 12 h. The experiments were conducted at: T = -1 °C, T = -5 °C, T = -10 °C and T = -20 °C. The hydrostatic load increments were maintained until the displacement changes were<0.01 mm. The observed variation of the void ratio (e) against the mean stress (p) is shown in Fig. 2a.

Perhaps the more notable effect of freezing temperature on soil behavior is the increase of the apparent pre-consolidation pressure (p_0) with the decrease of temperature. The arrows in Fig. 2a indicate the value of p_0 estimated at different temperatures. Fig. 2b presents the variation of the apparent pre-consolidation pressure with freezing temperature and cryogenic suction. Note that through Equation (1), it is possible to relate T with s. The temperature also affects the slope of the virgin consolidation curve, with a clear tendency to increase the stiffness of the frozen soil as the temperature decreases. No major effect of freezing temperature on the elastic slope (i.e., for pressures below p_0) is observed in these tests.

We may think that the observed increase in frozen-soil stiffness can be related to a possible increase in the ice stiffness as temperature decreases. The elastic properties of ice generally depend on ice formation type, strain rate, and water salinity. However, their mechanical properties do not depend (at least strongly) on (subzero) temperatures. For

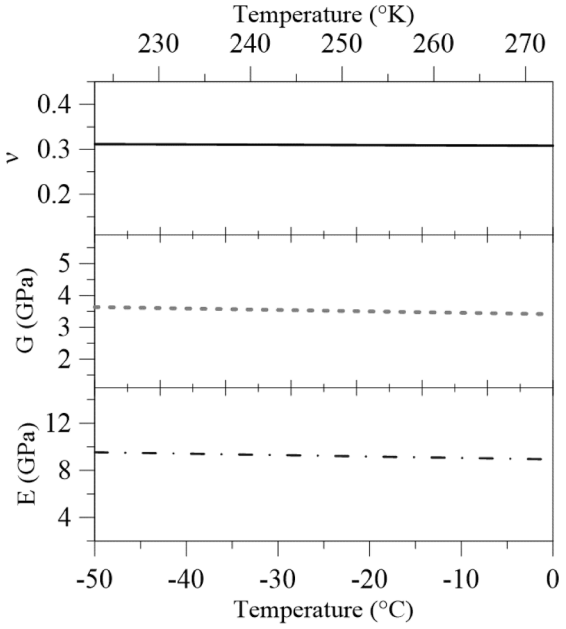

Fig. 3. Effect of temperature on ice elastic properties: E (Young's modulus), G (shear modulus), and Poisson's ratio Sinha et al. (1989).

example, Fig. 3 presents the variation of Young's and shear moduli (E and G, respectively) and Poisson's ratio (ν) for temperatures ranging from 0 to −50 °C (Sinha 1989). It can be observed that the impact of freezing temperature on elastic properties of ice is not significant and, therefore, it is possible to relate the increase of frozen soil stiffness and strength with the amount of unfrozen water in the frozen soils.

The effect of freezing temperature and confinement on soil strength has been reported in several publications (e.g., Arenson et al. 2004; Chen et al. 2020; Ma and Chang 2002; De Guzman et al. 2018; Beier and Sego 2008; Parameswaran and Jones 1981; Parameswaran 1980; Sayles 1974; Wang et al. 2018; Xu et al. 2019; Yamamoto and Springman 2014; Yang et al. 2010; Chuvilin et al. 2018; Zhang et al., 2016a; 2016b; 2016c; Zhao et al. 2020; Zheng et al. 2010; Zhu et al. 2020; Da Re et al. 2003; Esmaeili-Falak et al. 2018; Esmaeili-Falak et al. 2020; Czurda and Hohmann 1997; Kim et al. 2018; Liu et al. 2020; Liu et al. 2019). For example, Parameswaran (1980) and Parameswaran and Jones (1981) reported shearing tests on Ottawa sand at different sub-zero temperatures under unconfined conditions (Fig. 4a) and at different confining pressures maintaining a constant temperature of T = −10 °C (Fig. 4b),

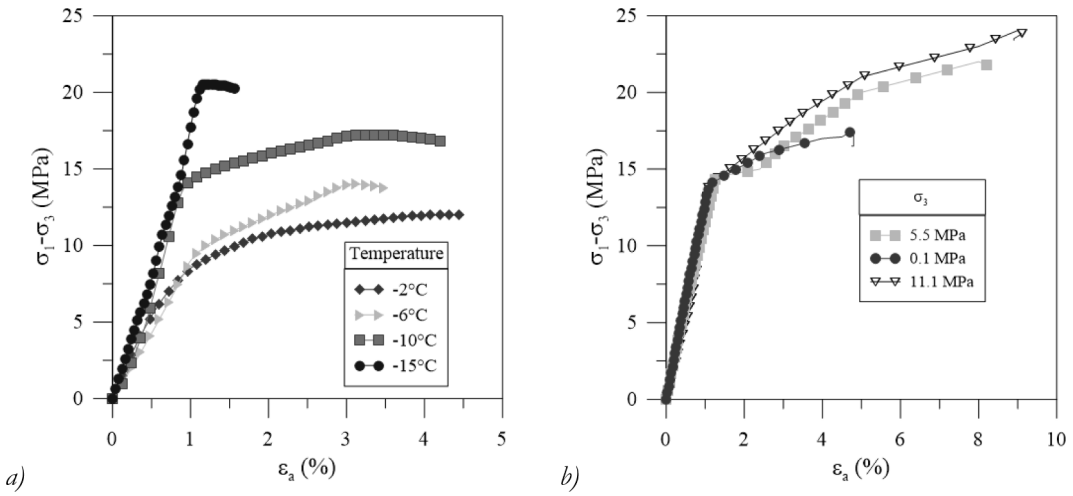

Fig. 4. Stress–strain behavior of reconstituted soils: a) effect of temperature (data from Parameswaran 1980), and b) effect of confining pressure (data from Parameswaran and Jones 1981).

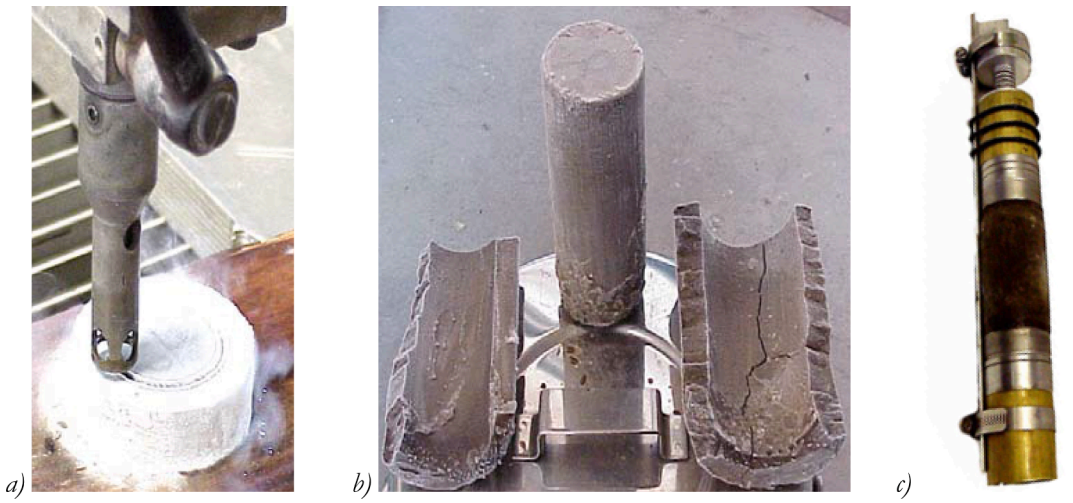

Fig. 5. a) Water-jet cutting of cylindrical specimen from the frozen soil core; b) frozen soil sample, c) spring-loaded V-block apparatus used to mount the end-caps to the frozen soil specimen.

respectively. These tests were conducted at a strain rate $\sim 7.7 \times 10^{-5}\,s^{-1}$. The samples were prepared at a dry density of around 1700 kg/m^3 and the gravimetric water content was about 20%. The freezing temperature has a marked impact on soil shear strength (with a tendency to increase it with the reduction of temperature) and a relatively minor influence on soil stiffness. As expected, the strength of the frozen soil increases with the confinement (Fig. 4b).

3. Tests on natural frozen soils

Tests on undisturbed frozen soil samples from Alaska were conducted at Sandia National Laboratory (SNL, Lee et al., 2002). The aim was to investigate the shear and volumetric behavior of natural frozen soils.

3.1. Material and methods

The soil samples were gathered from the FTU-11-18 and FTU-11-24 sites in the Yukon Test Range at Eielson Air Force Base in Alaska. The water table is shallow because of an adjacent creek. The sampling was conducted using a coring auger kit of 7.6 cm diameter. The length of the core was about 80 cm. The samples were extracted from a depth ranging from 0.2 m to 0.8 m below the ground level. The dominant soil type is silty clay. Most of the shallower samples (i.e., between 0 and 0.3 m) had a lower dry density (i.e., $\rho_d \sim 1.0$ g/cm^3) than the deeper ones (i.e., $\rho_d \sim 1.3$ g/cm^3). The water content of the samples varied from 34% to 85%, with most samples having a water content of around 40%. Variations in samples density and water content values are expected in natural soils, which will induce slight variations in the mechanical behavior of the material (as shown in Section 5.1).

After extracting the cores, they were transported in a cooler to SNL and stored in a freezer at –10° C. A water-jet cutting technique was used to extract smaller diameter core specimens from the 7.6 cm core. The water-jet cuts the specimen using the stream of high-pressure water, mixed with abrasives exiting the small diameter nozzle. A nozzle with a 0.03 cm orifice in diameter was used. Fig. 5a shows the water jet coring used for preparing a cylindrical specimen from frozen soil cores. Fig. 5b corresponds to a picture of the frozen soil sample after cutting it. No air inclusions were observed in this material. The extracted sample was then cut perpendicular to the longitudinal axis of the core, using a diamond saw cooled by liquid nitrogen. We used a spring-loaded V-block design (Fig. 5c), based on the principle of pressure melting, to ensure the ends of the cylindrical specimens were prepared perpendicular to the axis of the specimen and parallel to each other. The specimen

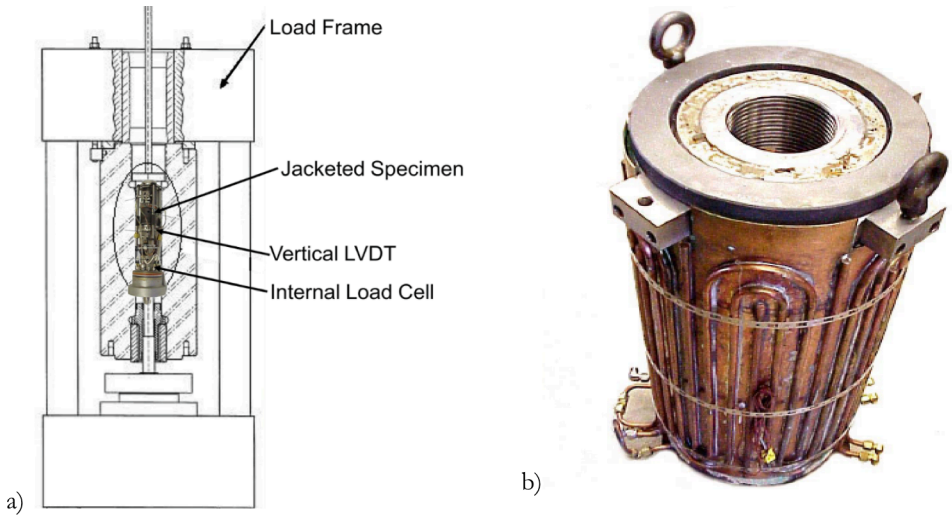

Fig. 6. Experimental set up: a) High-Pressure Low Temperature (HPLT) cell; b) pressure vessel with circulating cooling system comprising the test cell (Lee et al., 2002).

Table 1
Natural samples testing conditions.

Test type	Temperature testing range [° C]	N°. of tests analyzed	Test Control
Hydrostatic compression	−6 to −25.6	8	Pressure control 0.03 MPa/s
Uniaxial compression	−4.7 to 23.7	2	Strain control 10^{-4} to 10^{-1} s^{-1}
Deviatoric compression	−6 to −26	15	Strain control 10^{-4} s^{-1}

was mounted between the cylindrical endcaps and the assembly was placed on the V-block. The spring-loaded clamp applies the axial force to the specimen. The pressure melting occurs between the ends of the specimen and the endcaps. This system allowed the frozen soil specimen to be mounted with its ends parallel to each other and perpendicular to the vertical axis.

Once the individual cores were prepared, they were jacketed with neoprene sleeves, which remained flexible under the cold temperatures of interest. The cold temperatures and concomitant piston-seal friction required the use of internal load cells. Two load cells were designed for operation under sub-zero conditions. The instrumented sample and pressure vessel configuration for testing are shown in Fig. 6a. A unique High-Pressure Low Temperature (HPLT) vessel with an external cooling system based on liquid nitrogen circulation was developed (Fig. 6b). The assembled vessel was then placed into a 1.9 MN servo-controlled load frame. Up to twelve piezoelectric acoustic velocity pins were affixed to the sample using low-temperature epoxy to enable P- and S-waves velocity determination during the testing and record the onset of plastic straining via acoustic emissions, but these results are not discussed here. More information about the set-up and equipment used can be found in Lee et al. (2002).

Several quasi-static tests were conducted on the samples to estimate the material properties. Table 1 lists the various tests performed under varying temperature and load conditions. A brief discussion about these tests is presented in the next section.

3.2. Hydrostatic Behavior

After preparing the cylindrical specimens (according to the ASTM D4543), the jacketed samples were instrumented with linear variable differential transformer (LVDT) sensors, and the assembly was inserted into the test cell. The push rod, typically used for applying the axial load to the specimen, was pulled back to avoid initial contact with the top of the sample configuration during initial assembly. In this configuration, no deviatoric stress was applied to the specimens during testing. The confining pressure (p) was increased all around the specimens using a confining fluid composed of light hydrotreated petroleum distillate. The

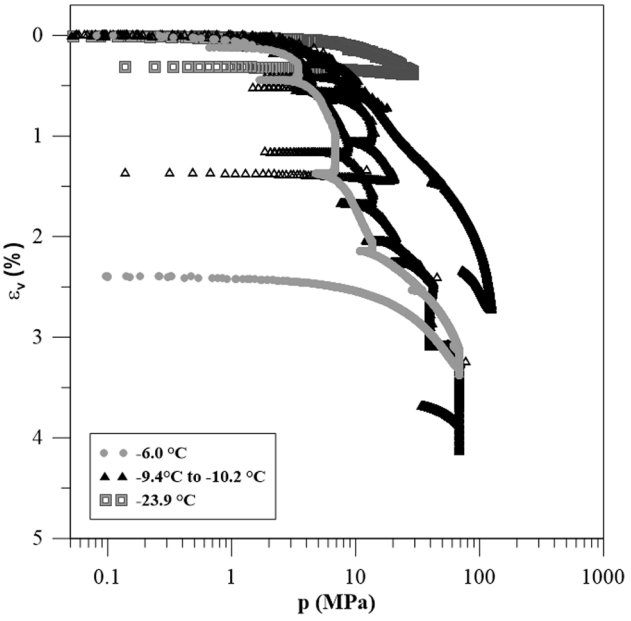

Fig. 7. Isotropic behavior of natural frozen soils at different temperatures.

Table 2
Apparent preconsolidation mean stress at different freezing temperatures.

Temperature (°C)	Preconsolidation mean stress (MPa)
−23.9	10.3
−10.5	4.8
−10.4	4.6
−10.2	4.0
−9.4	3.8
−6.0	2.3

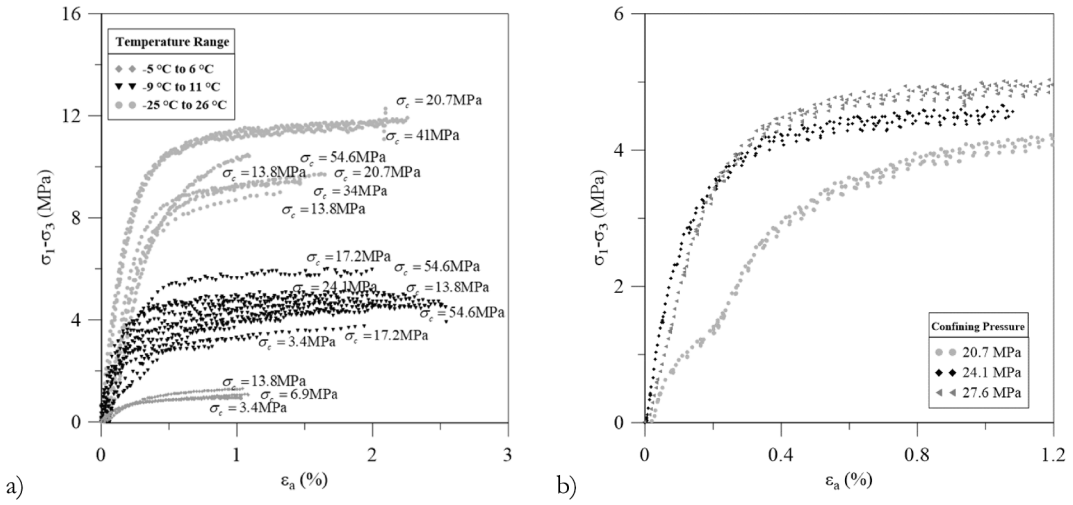

Fig. 8. Shear behavior of natural frozen soils: a) effect of temperature, and b) effect of confining pressure on tests conducted at T = -10 °C.

pressure was measured by means of pressure transducers connected to the HPLT test cell. Vertical and horizontal LVDTs were used to measure the axial and lateral displacements, respectively.

The hydrostatic behavior of the frozen soil samples in terms of void ratio versus mean net stress at different temperatures is shown in Fig. 7. There is a clear increase in pre-consolidation pressures with the decrease in temperature (see Table 2). There is also a marked effect of the temperature on the virgin consolidation slope. The variation of the pre-consolidation pressure with freezing temperature and frozen soil stiffness is qualitatively similar to the one observed in reconstituted frozen samples (Section 2.2). It is assumed here that the additional 'bonding' provided by the increase of cryosuction (i.e., as the temperature decreases) is the primary phenomenon behind the increase of preconsolidation pressure and stiffness, in both natural and reconstituted samples. A similar behavior is observed in unsaturated soils, where the increase of matric suction is associated with the increase of the preconsolidation pressure, stiffness, and strength. In the following Sections, we present the evolution laws that incorporate the effect of cryonic suction on key mechanical properties of permafrost soils.

3.3. Shear Behavior

Triaxial tests were conducted under different temperatures and confining pressures. After the specimen assembly was placed in the test cell, the hydraulic pressure was applied up to a predetermined level of confinement. Upon stabilizing the confining pressure, the specimen was loaded axially by applying the deviatoric stress (i.e., the difference between the axial and radial stresses: $q = \sigma_1\text{-}\sigma_3$). Fig. 8a and 8b show the effect of temperature and confining pressure (tests conducted at T = -10 °C), respectively, on the strength of natural frozen soils. The specimens exhibit trends similar to those observed in the reconstituted soils, showing a significant increase of frozen soil strength with the decrease of temperature. The impact of confining pressure on soil strength is less relevant, but follows the expected behavior, showing an increase in strength with the increase in the confining pressure. We also carried out unconfined uniaxial tests in a 0.1 MN servo-controlled loading machine. After preparing the samples (as explained in Section 3.1), the specimens were loaded at a constant displacement rate of 10^{-3} mm/s corresponding to a strain rate of 10^{-5} s^{-1}. The tests were conducted until an axial strain of around 3% was reached, by which point the sample deformation had experienced a near-plateau or very slight strain hardening evidenced by the stress–strain curves. On the basis of this plateau behavior, the tests were terminated. In Sections 5.2 and 5.3 the analyses of the experiments are presented in more detail together with the modeling results.

4. Mathematical framework for modeling frozen soils behavior

In this Section we present the mechanical constitutive model adopted in this work to analyze the behavior of the natural frozen soil samples discussed above, followed by a brief introduction of the adopted THM formulation and computer code we used to analyze the behavior of frozen soils.

4.1. Mechanical constitutive model for frozen soils

The constitutive model adopted in this work is based on the elasto-plastic model for frozen soil proposed by Nishimura et al. (2009). The formulation extends the Modified Cam-Clay Model (MCCM) to account for the effect of changes in temperature and cryogenic suction in soils (Nishimura et al. 2009). The approach is inspired by the Barcelona Basic Model (BBM) proposed by Alonso et al. (1990) to describe the mechanical behavior of unsaturated soils. The BBM can reproduce the increase of the preconsolidation pressure, stiffness, and shear strength with the increase of suction. Considering that Equation (2) relates subzero temperature with cryogenic suction, the effect of subzero temperatures on frozen soils behavior can be equally described in terms of cryogenic suction (e.g., as shown in Fig. 2b). It is also worth mentioning that the BBM is particularly well suited to reproduce the volumetric collapse compression behavior of unsaturated soils observed upon wetting. A similar response is observed in frozen soils subjected to thawing (i.e., cryogenic suction decrease).

The model considers two stress variables to describe the mechanical behavior of frozen soils, namely, the net stress (σ_n [N/m^2]) and the cryogenic suction. The net stress is defined as follows (Nishimura et al., 2009):

$$\sigma_n = \sigma - \max(P_l, P_i, 0) \tag{3}$$

where σ [N/m^2] is the total stress.

Nishimura et al. (2009) assumed that the MCCM governs the behavior of unfrozen soils. In this paper, we replaced the elliptical Yield Surface (YS) assumed in the MCCM with the Hierarchicl Single Surface (HiSS) proposed by Desai et al. (1986; 1989). We also included sub-loading concepts into the model formulation (Hashiguchi, 1989; Hashiguchi and Ueno, 1977). Nishimura et al. (2009) model predicts a sharp transition between over-consolidated and normally-consolidated states, a feature of soil behavior that was not observed in the natural frozen soils investigated in this work (e.g., Figs. 6 and 7). We also found difficulty in describing the shearing behavior of natural frozen soils using the elliptical YS adopted in the Nishamura et al. (2009). Therefore,

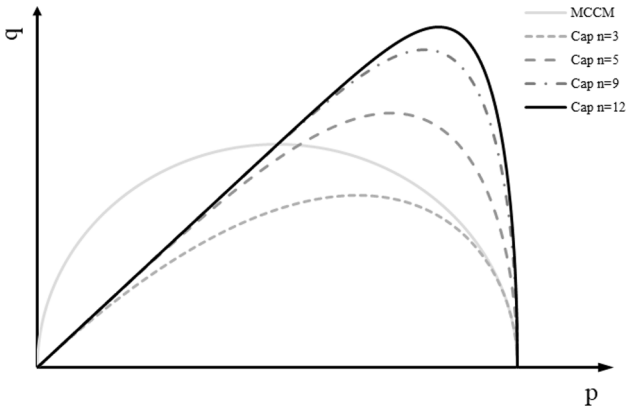

Fig. 9. Different HISS yield surface shapes.

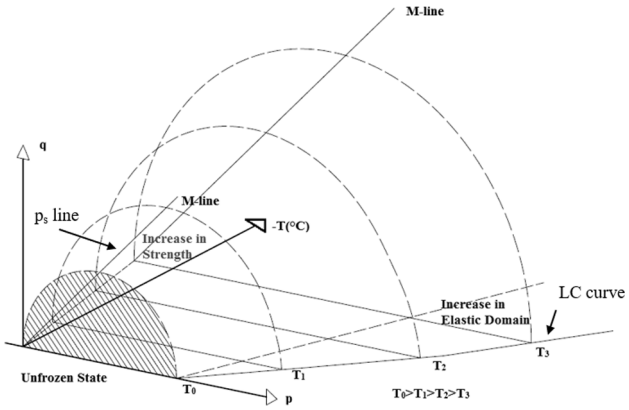

Fig. 10. Schematic representation of the 3D yield surface for frozen soils.

we propose in this work to use a HiSS sub-loading model to provide a more general and versatile constitutive model to describe frozen soil behavior. This type of model has been used with success to model other complex soils behaviors (e.g., Romero et al. 2019; Gai and Sánchez, 2017; 2019). The HiSS framework involves a single and continuous yield surface that can adopt different shapes depending on the selected parameters. The equation defining the yield surface (F = 0) is given by:

$$F = \frac{\alpha q^2}{M^2} - \gamma 3^2 p_n^2 + \gamma 3^2 p_n \left[R\left(\frac{p_{n0} - p_s}{2}\right) \right]^{2-n} \tag{4}$$

where M [dimensionless] is the slope of the critical state line in the p-q space; p_s [N/m^2] is related to the increase in soil strength with the decrease of temperature (or increase of the cryogenic suction); and p_{no} [N/m^2] is the preconsolidation pressure for frozen states at a given temperature. The dimensionless parameters n, α, and γ are constants that define the shape of the yield surface. Some examples of possible shapes of the yield surface are shown in Fig. 9. *R* [dimensionless] is the sub-loading ratio (with $0 < R < 1$). The evolution of the sub-loading ratio *R* is expressed as follows:

$$dR = -\eta \ln R |d\varepsilon^p| \tag{5}$$

where $d\varepsilon^p$ [dimensionless] is the increment of the total plastic strain; and η [dimensionless] is a parameter that controls the sub-loading rate.

The critical state model is extended to frozen soils by expanding the size of the yield surface as the freezing temperature decreases (or the cryogenic suction increases). This model feature considers the increase of both pre-consolidation pressure and soil strength with the decrease of temperature. The increase of pre-consolidation pressure induced by a cryogenic suction increase is accompanied by an expansion of the elastic domain, which is controlled by the following expression:

$$p_{n0} = p_c \left(\frac{p_0^*}{p_c}\right)^{\frac{\lambda_0 - \kappa}{\lambda_{(s)} - \kappa}} \tag{6}$$

where p_0^* [N/m^2] is the pre-consolidation pressure for saturated (unfrozen) states; p_c [N/m^2] is a model parameter; κ [dimensionless] is the elastic stiffness parameter for changes in mean net stress; and $\lambda_{(s)}$ [dimensionless] is the compressibility parameter for changes in mean net stress for virgin states of soil for frozen states calculated as follows:

$$\lambda_{(s)} = \lambda_0 [r + (1 - r)\exp(-\beta s)] \tag{7}$$

where λ_0 [dimensionless] is the slope of virgin state for saturated (unfrozen) conditions; β [dimensionless] is a model parameter that controls the rate of increase of soil stiffness with cryogenic suction; and r [dimensionless] is the model parameter that defines the minimum soil compressibility. For example, Fig. 2b presents the trace of the yield surface on the p-s plane (obtained after combining Eqs. (5) and (6)) for the soil used by Qi et al. (2010). This curve is termed the Load-Collapse (LC) curve, because yielding is predicted when the soil is loaded beyond this curve, and collapse plastic compression strains are computed when thawing.

The expansion of the yield surface required to capture the increase in soil strength with the decrease of temperature is modeled through the variable p_s, as follows:

$$p_s = ks \tag{8}$$

where k [dimensionless] is a model parameter that controls the increase of strength with cryogenic suction. A three-dimensional representation of the yield surface in the p-q-T (or p-q-s) space is shown in Fig. 10.

In line with the MCCM, it is assumed that the hardening of the material depends on the plastic volumetric strains increment ($d\varepsilon_v^p$), through the following equation:

$$dp_0^* = \frac{(1 + e)}{(\lambda_0 - \kappa)} p_0^* d\varepsilon_v^p \tag{9}$$

The soil elastic bulk modulus is calculated as follows:

$$K_p = \frac{1 + e}{\kappa} p_n \tag{10}$$

The elastic shear modulus G is determined using the following expression where ν is the Poisson's Ration (assumed constant):

$$G = \frac{3(1 - 2\nu)}{2(1 + \nu)} K_p \tag{11}$$

4.2. Mathematical formulation

The adopted approach to model the behavior of frozen soils is based on the extension to freezing temperatures of an existing framework (Olivella et al. 1994, 1996). The formulation is composed of three main components: i) balance equations, ii) constitutive equations, and iii) equilibrium restrictions (i.e., Eq. (1)). Full details about the basic mathematical framework and numerical code can be found in Olivella et al. 1994 and Olivella et al. 1996, respectively. A brief discussion of the main components of the mathematical approach is presented below.

4.2.1. Balance equations

The water mass balance equation is expressed as:

$$\frac{\partial}{\partial t}(\rho_l S_l \phi + \rho_i S_i \phi) + \nabla.(\rho_l \mathbf{q}_l) = f^w \tag{12}$$

where S_l [dimensionless] and S_i [dimensionless] are the partial saturation of unfrozen-water (liquid) and ice phases, respectively; ϕ [dimensionless] is the porosity, $\mathbf{q}_l$ [m/s] is the liquid water flux and f^w [g/(m^3·s)] is the sink/source term of water.

The solid mass balance equation is written as follows:

$$\frac{\partial}{\partial t}[\rho_s(1-\phi)] + \nabla.[\rho_s(1-\phi)\boldsymbol{v}] = 0 \tag{13}$$

where ρ_s [g/m^3] is the density of the solid particles, and **v** [m/s] is the soil movement relative to the fixed reference frame.

The internal energy balance equation is written as:

$$\frac{\partial}{\partial t}[e_s\rho_s(1-\phi) + e_l\rho_l S_l\phi + e_i\rho_i S_i\phi] + \nabla.\left(-\lambda\nabla T + j_l^e\right) = f^e \tag{14}$$

where e_s [J/g], e_l [J/g] and e_i [J/g] are the specific internal energies associated with the soil minerals, liquid–water, and ice, respectively; j_l^e[W/m^2] is the advective term of heat flux associated with the movement of the liquid phase; λ [W/(m·K)] is the thermal conductivity of the porous medium; and f^e [W/m^3] is the term associated with any sink or source of energy. Energy consumption or liberation associated with ice formation/fusion is considered using the corresponding latent heats. Therefore, the formulation inherently captures energy changes during endothermic or exothermic processes through specific internal energies and the corresponding changes in volume fractions S_l, and S_i.

The balance of momentum equation for the porous medium reduces (if inertial terms are neglected) to the equilibrium equation for total stresses:

$$\nabla\bullet\sigma + \mathbf{b} = 0 \tag{15}$$

where σ is the total stress tensor and **b** [N/m^3] is the body forces vector.

4.2.2. Constitutive equations for the thermal and hydraulic problems

The constitutive equations relate the main unknowns (i.e., liquid pressure, temperature, and displacement field) to the dependent variables (e.g., liquid and heat fluxes, strains, degree of liquid saturation).

Conductive heat flow: Fourier's law governs the heat flow $\mathbf{i_c}$ [W/m^2], for three-dimensional flow conditions and isotropic thermal conductivity,

$$\boldsymbol{i}_c = -\lambda\ \nabla T \tag{16}$$

A thermal conductivity model based on the geometric mean of the thermal conductivities of the three phases was adopted (CODE_BRIGHT 2021):

$$\lambda = \lambda_s^{(1-\phi)}\lambda_l^{\phi S_l}\lambda_i^{\phi(1-S_l)} \tag{17}$$

where λ_s, λ_l and λ_i are the thermal conductivities of the solid, liquid, and ice phases, respectively.

Advective Liquid Flow: the generalized Darcy's law governs the advective fluxes [m/s] of the unfrozen water in soils:

$$\boldsymbol{q}_l = -\boldsymbol{K}_l(\nabla P_l - \rho_l\boldsymbol{g}) \tag{18}$$

where **g** the gravity vector (i.e., the scalar g = 9.8 m/s^2 times the vector [0,0,1]^T). The tensor $\mathbf{K_l}$ [m^4/(N s)] captures the frozen soil permeability for the liquid phase in a three-dimensional flow. The permeability $\mathbf{K}_\alpha$ depends on the sediment intrinsic permeability **k** [m^2]; liquid μ_l dynamic viscosity [N s/m^2]; and relative permeability k_{rl} [dimensionless]:

$$\boldsymbol{K}_l = \boldsymbol{k}\frac{k_{rl}}{\mu_l} \tag{19}$$

If the medium is isotropic, $\mathbf{K_l}$ is the scalar permeability k_l times the identity matrix **I**. The intrinsic permeability of the frozen soil is estimated from the intrinsic permeability in the medium without ice (k_o) determined at the reference porosity (ϕ_o) based on a generalized Kozeny-Carman model:

$$k = k_0\frac{\phi^3}{(1-\phi)^2}\frac{(1-\phi_0)^2}{\phi_0^3} \tag{20}$$

The relative permeabilities for liquid $k_{r\ell}$ increase as S_ℓ increases. A power function was adopted in this work:

$$k_{r\ell} = (S_\ell)^m \tag{21}$$

where m is a model parameter. The adopted permeability law is relatively simple. More advanced models (as the ones suggested in Teng et al. 2021) can be implemented, if necessary.

The interfacial tension between liquid and ice sustains the difference between the liquid and ice pressures. To compute the degree of saturation of unfrozen water at any given temperature, the modified van Genuchten model is adopted (Nishimura et al. 2009):

$$S_l = \left(1 + \left(\frac{-\left(1-\frac{\rho_i}{\rho_l}\right)P_l - \rho_i l\,\ln\left(\frac{T}{273.15}\right)_i}{P}\right)^{\frac{1}{1-\lambda}}\right)^{-\lambda} \tag{22}$$

where P and λ are model parameters that control the shape of the unfrozen-water retention curve.

Liquid-to-ice and ice-to-liquid water phase changes: it is assumed that ice thawing/formation phenomena are fast equilibrium-controlled reactions (i.e., the phase-change characteristic time is much smaller than the characteristic times related to other processes in soils, such as diffusion, advection, or conduction. This implies that when the current pressure and temperature are favorable for the phase change, the process takes place instantaneously. In this formulation, the amount of water involved in the phase transition is controlled by equation (22) that relates fluid pressures, temperature, and unfrozen water saturation. CODE_BRIGHT has been recently upgraded to simulate phase transformations in soils (including ice melting and formation) using a novel, non-equilibrium, pseudo-kinetic approach (Teymouri et al., 2020), which can be used for those analyses in which it is crucial to simulate the time involved in the phase transformation process.

4.3. Computer code

The finite element program CODE_BRIGHT (Olivella 1996; CODE_BRIGHT 2021) was updated with the equations for frozen soils described above. CODE_BRIGHT is a numerical tool developed to solve coupled thermo-hydro-mechanical problems in geological media. This program has been widely validated and used to solve different problems in geological media (e.g., Gens et al. 2009; Sánchez et al., 2014, 2016; Gens, 2010). One main unknown (or state variable) is related to each balance equation, e.g., displacement field (**u**), P_l, T, ϕ are associated with the momentum, water-mass, energy, and solid balance equations, respectively. From state variables, the dependent variables (e.g., σ, S_l , **i**, $\mathbf{q_l}$) are calculated using the constitutive equations. Clausius-Clapeyron equation (1) is used to calculate P_i base on P_l, T, and phase densities. The unknowns are obtained by solving the system of partial differential equations numerically in a fully coupled way, simultaneously. The Galerkin finite element method is used for spatial discretization and finite differences are adopted for temporal discretization. The discretization in time is linear. and an implicit scheme is adopted. The program has an automatic discretization of time. More details can be found in (Olivella et al. 1996).

5. Applications

The mechanical model presented in Section 4.1 is used first to describe the behavior of the natural frozen soil observed in the experiments. Finally, the upgraded computer code is applied to solve a problem of practical engineering relevance.

5.1. Modeling the mechanical behavior of natural frozen soils

The tests conducted on frozen soil samples at SNL provide an

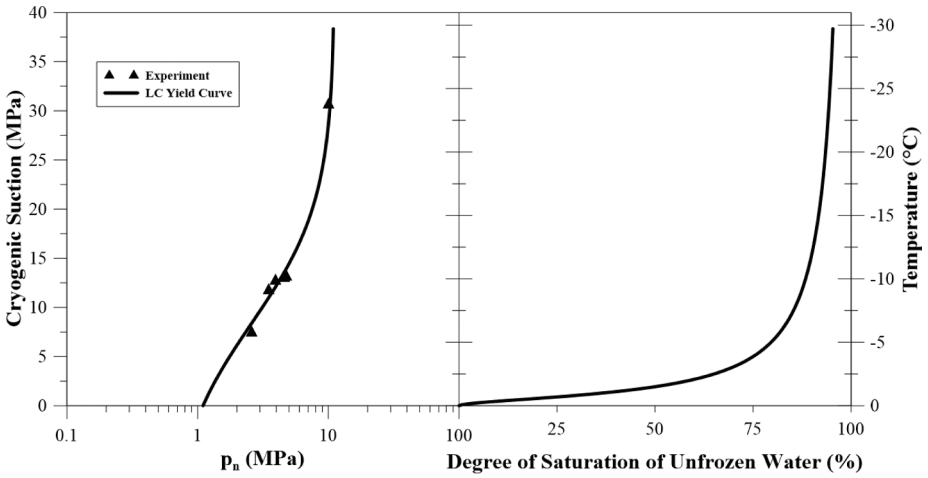

Fig. 11. LC yield curve on the isotropic plane mean-net-stress - temperature/cryogenic-suction (left plot) and soil unfrozen-water retention curve (right plot).

Table 3
Mechanical model parameters used for natural samples.

Symbol	Parameter	Value	Symbol	Parameter	Value
Isotropic behavior					
κ	elastic stiffness parameter for changes in mean net stress	0.0001	ν	Poisson's ratio	0.35
$\lambda_{(0)}$	compressibility parameter for changes in mean net stress for virgin states of soil	0.028	p_o*	net mean yield stress for saturated conditions	1.1 [MPa]
r	parameter controlling soil compressibility	0.21	β	parameter controlling soil compressibility	0.16
p_c	reference stress	0.6 [MPa]			
Shearing behavior					
M	slope of the critical state line	0.07	k	constant describing the increase of strength with cryogenic suction	0.41
HiSS YS and Sub-loading parameters					
α	HiSS YS constant	3	γ	HiSS YS constant	1/9
n	HiSS YS constant	12	η	constant controlling the sub-loading rate	100

excellent opportunity to check the capability of the elasto-plastic model to describe the real behavior of this type of soil. We selected some tests to determine the model parameters and reserved some of them to validate the proposed approach. Despite the variations in sample density discussed in Section 3.1, a single set of model parameters were assumed to model all the experiments. The main interest of this work is not to precisely reproduce the experimental observations, but to check whether or not the proposed mechanical model and formulation are able to capture qualitatively well the main tendencies and features observed in the experiments involving natural frozen soils. Furthermore, based on the shallow water table condition observed at the site (i.e., Section 3.1) and that air inclusions were not apparent in this material (i.e., Fig. 5b), we assumed that the samples are water-saturated, with the pores filled by ice, or by liquid water, or by a combination of them.

We analyzed first the isotropic tests conducted at T = −6 °C, T = −10.4 °C, and T = −23.9 °C to estimate the parameters controlling the behavior of frozen soils in the e – p_n plane. The proposed LC curve for the Alaska frozen soil is depicted in Fig. 11a and the corresponding model parameters are listed in Table 3. Fig. 11b presents the adopted soil unfrozen-water retention curve in terms of the liquid saturation according to equation (22).

Fig. 12 presents the comparisons between the experimental data and the corresponding model outputs. We used the loading for over-consolidated conditions and the unloading path (Fig. 11c) to determine κ. We estimated the parameters involved in the LC curve (Equations (5) and (6)) using the values of p_o and λ(s) at different temperature We included the results obtained from both, the adapted BBM (i.e. as suggested in Nishimura et al., 2009), and the model introduced in Section 4.1 that incorporates sub-loading concepts. It can be seen that the BBM predicts a sharp transition between elastic and plastic states. In contrast, the sub-loading model properly describes the actual smooth elastic–plastic transition behavior observed in this material.

We adopted the three remaining isotropic tests to check the model performance, namely T = −9.4 °C; T = −10.2 °C; and T = 10.5° °C. The proposed model with the selected parameters is able to satisfactorily capture the experimental observations from these tests as well (see Fig. 13).

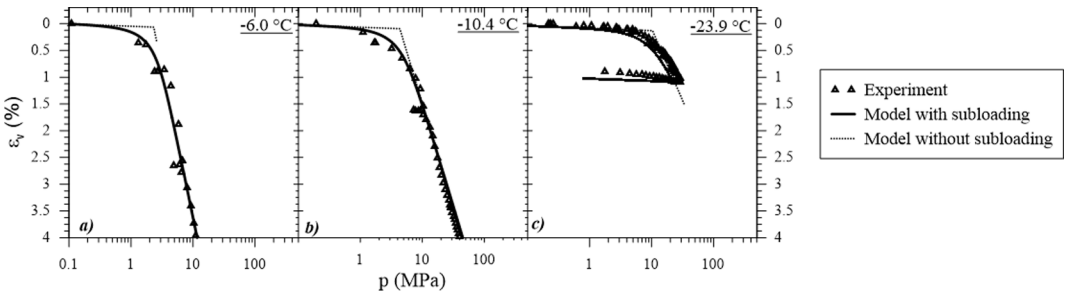

Fig. 12. Experimental and modeling results of isotopic tests at three temperatures: a) T = -6 °C; b) T = -10.4 °C; and c) T = –23.9 °C.

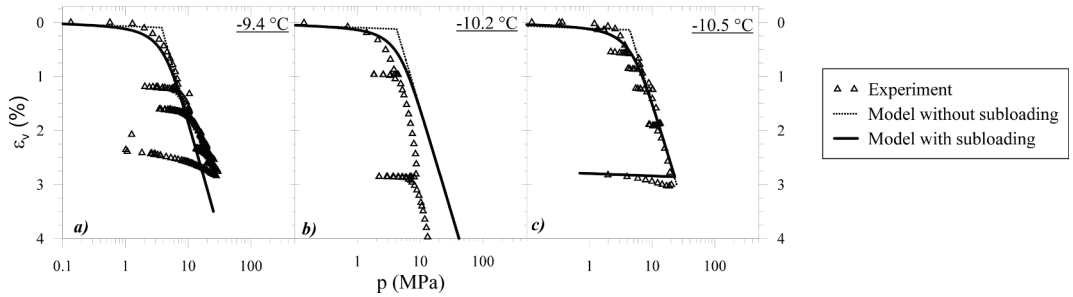

Fig. 13. Experimental and modeling results of isotopic tests at three temperatures: a) T = -9.4 °C; b) T = -10.2 °C and c) T = -10.5 °C.

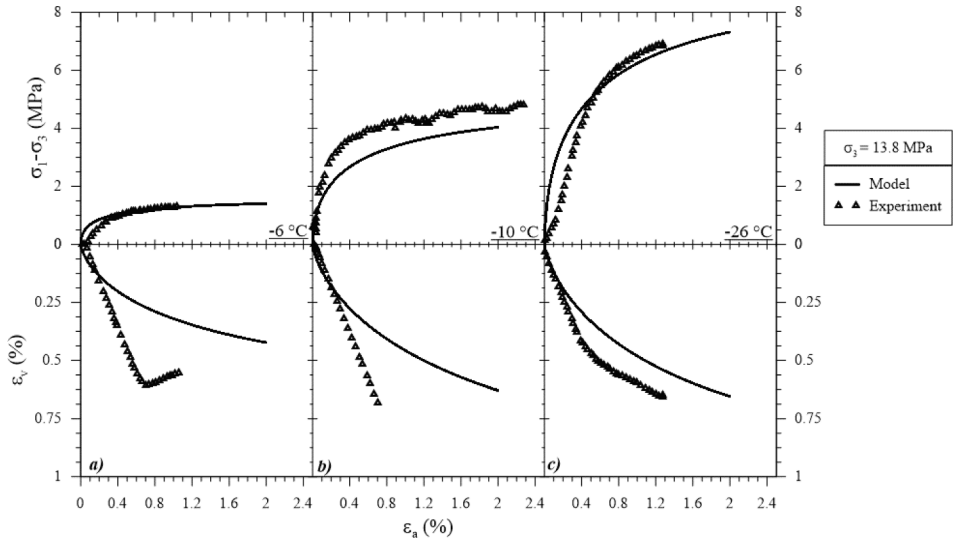

Fig. 14. Effect of freezing temperature. Model and experimental results in terms of deviatoric stress and volumetric strains versus axial strain. Triaxial tests at a constant cell pressure σ_3 = 13.8 MPa, and at three temperatures: a) T = -6 °C; b) T = -10 °C; and c) T = -26 °C.

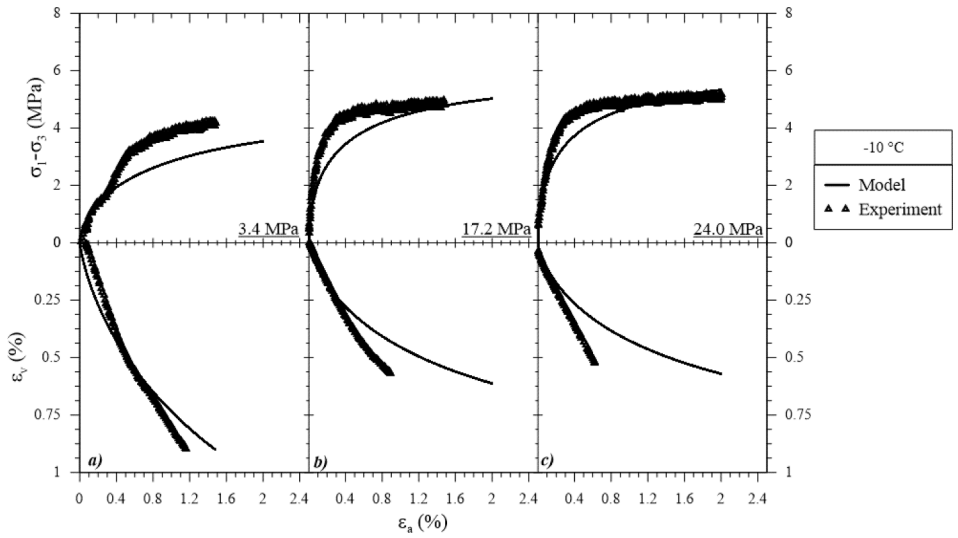

Fig. 15. Effect of confinement. Model and experimental results in terms of deviatoric stress and volumetric strains versus axial strains. Triaxial tests at a constant temperature T = -10 °C and at three cell pressures: a) σ_3 = 3.4 MPa; b) σ_3 = 17.2 MPa; and c) σ_3 = 24 MPa.

Figs. 14–16 present the triaxial tests we selected to calibrate the model parameters together with the corresponding simulations. Fig. 14a, 14b, and 14c correspond to experiments conducted at the same confinement (σ_3 = 13.8 MPa), and at three temperatures: T = −6 °C; T = −10 °C; and T = −26 °C, respectively. The effect of freezing temperature on shear behavior is notorious, with a tendency for the shear strength to increase as the temperature reduces. Fig. 15a, 15b and 15c group the tests conducted at a constant temperature T = −10 °C; and at three confinements, σ_3 = 3.4 MPa; σ_3 = 17.2 MPa; and σ_3 = 24 MPa, respectively. Fig. 16a, 16b and 16c group the tests conducted at a

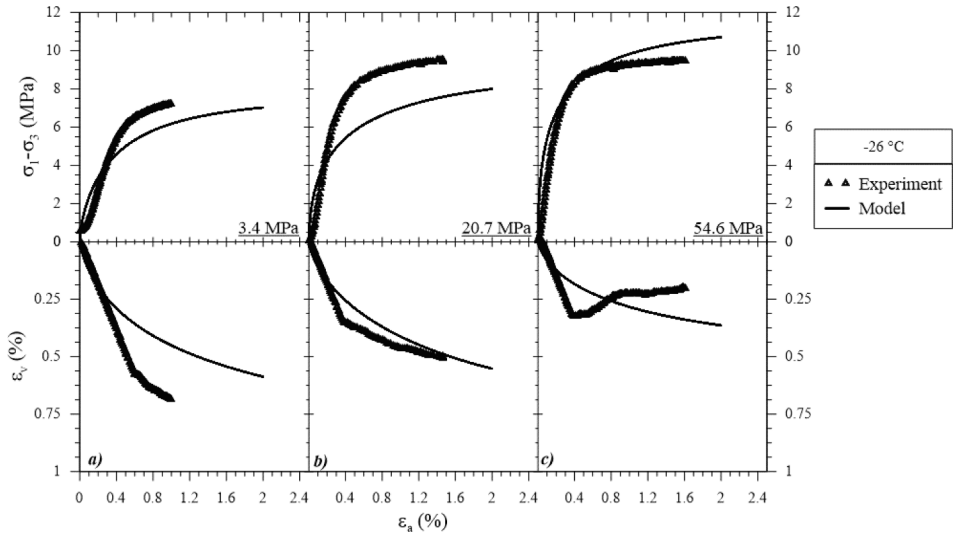

Fig. 16. Effect of confinement. Model and experimental results in terms of deviatoric stress and volumetric strains versus axial strains. Triaxial tests at a constant temperature of T = -26 °C, and at three cell pressures: a) σ_3 = 3.4 MPa; b) σ_3 = 20.7 MPa; c) σ_3 = 54.6 MPa.

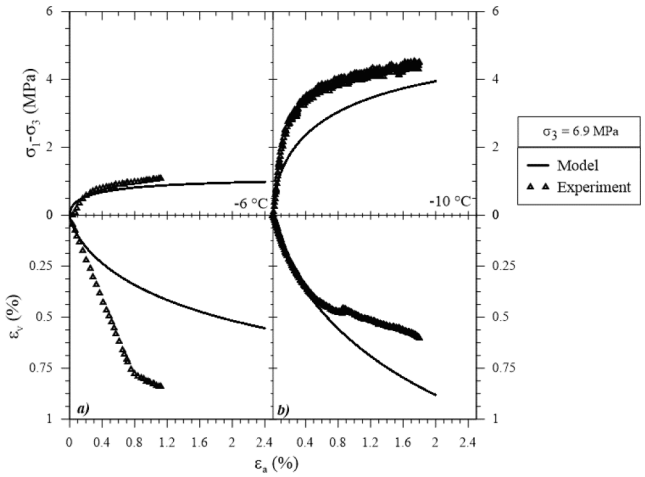

Fig. 17. Validation, model and experimental results in terms of deviatoric stress and volumetric strains versus axial strains obtained from the triaxial tests at σ_3 = 6.9 MPa, at two temperatures: a) T = –6 °C; and b) T = -10 °C.

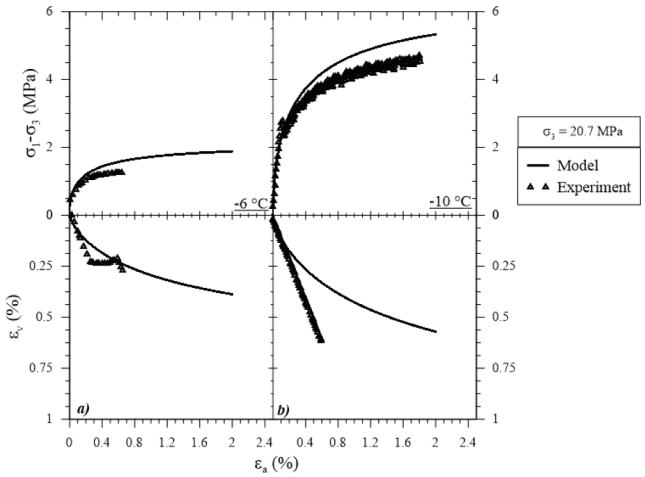

Fig. 18. Validation, model and experimental results in terms of deviatoric stress (top figures) and volumetric strains (bottom figures) versus axial strains. Triaxial tests at σ_3 = 20.7 MPa at two temperatures a) T = -6 °C.; and b) T = –10 °C.

constant temperature T = −26 °C; and three confinements, σ_3 = 3.4 MPa; σ_3 = 20.7 MPa; and σ_3 = 54.6 MPa, respectively. Figs. 15 and 16 show that the effect of confinement on shear strength is relatively minor. We used these tests (i.e., Figs. 15 and 16) to determine the model parameter M, and the experiments presented in Fig. 14 to determine the parameter k (which controls the increase of shear strength with cryonic suction, i.e., Equation (8)). We also used these nine tests (i.e., Figs. 14–16) to estimate (by back-calculation) the parameters associated with the shape of the yield surface (i.e., α, γ, and *n*). Table 3 lists the corresponding model parameters. We initially adopted the MCCM yield surface, but with the elliptical yield surface shape we were not able to properly capture the observed soil behavior.

We used other experiments we conducted on frozen soils to check the model performance. For example, Fig. 17 presents the simulation of two tests performed at the same confinement σ_3 = 6.9 MPa (which was not considered in the calibration tests), and at two temperatures: T = −6 °C, and T = −10 °C (i.e., Fig. 17a and 17b, respectively). Fig. 18 presents the modeling of two tests conducted at the same confinement σ_3 = 20.7 MPa, and at two temperatures: T = −6 °C, and T = −10 °C (i.e., Fig. 18a and 18b, respectively). Fig. 19 presents the simulation of two tests carried out at the same temperature T = -26 °C, and at two confinements: σ_3 = 7.2 MPa, and σ_3 = 34 MPa (i.e., Fig. 19a and 19b, respectively). Finally, Fig. 20 presents the modeling of unconfined tests performed at two temperatures: T = −10.2 °C and T = −25 °C (i.e., Fig. 19a and 19b, respectively).

Looking at isotropic and shearing tests, we can see that the model successfully captures the increase of the apparent pre-consolidation mean stress, soil stiffness, and strength with the decrease of temperatures in frozen soils. The model qualitatively captures the volume change observed in these tests as well. Most of the samples exhibit a clear volumetric compressive behavior upon shearing and the model simulated reasonably well the main trends observed in the tests. In Fig. 16c and 19b, the soil exhibits a sight dilatant behavior, which is not captured in this analysis. Note that volume changes upon shearing in frozen soils are challenging to measure. Experimental information in this regard is relatively scarce in the literature. Also, the experimentally observed smooth transition between elastic and plastic states is properly reproduced by the proposed model. Regardless of minor differences between simulated and experimental results, the overall performance of the model can be considered satisfactory, particularly considering that we are dealing with natural (heterogenous) samples and a huge range of

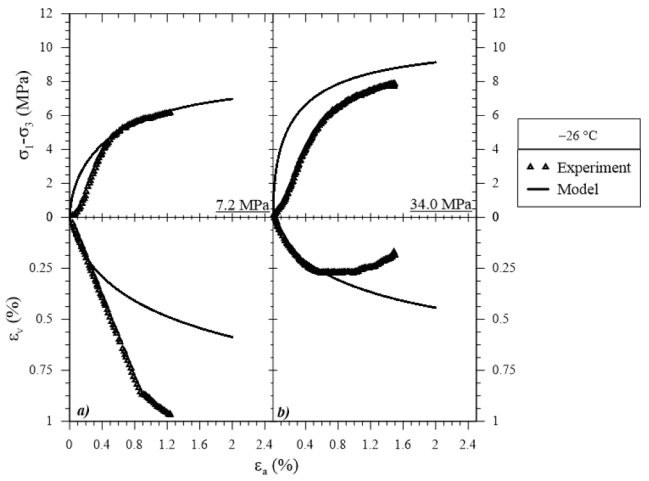

Fig. 19. Validation, model and experimental results in terms of deviatoric stress (top) and volumetric strains (bottom) versus axial strains. Triaxial tests at T = -26 °C, and at two cell pressures: a) σ_3 = 7.2 MPa; and b) σ_3 = 34 MPa.

temperatures (i.e., −6 °C < T < -26 °C) and confinements (i.e., 0 < σ_3 =< 54.6 MPa).

5.2. Modeling compression collapse phenomena in frozen soils

One of the key aspects of the constitutive model discussed above is its ability to replicate the volumetric collapse compression behavior observed when frozen soils are thawed at constant stress. This section deals with the application of the model to simulate a thaw-related failure, which can be relevant for structures constructed in arctic regions. We present an analysis based on the case discussed in Zhukov (1990). The work details the failure of an administrative service combine building of the Kadykchanskaya mine in the Magadan region of the former USSR built in 1967. The building foundation was constructed on an ice-covered soil base. The usage of utilities inside the structure leads to an excessive settlement resulting in cracks in the building. This caused a collapse in the soil structure, which was manifested in the form of cracks in the building structure, as shown in Fig. 21a. A possible stress path followed by this soil during heating at constant stress is schematically indicated in Fig. 21b. This implies that the ground undergoes significant (irreversible) volume changes during thawing at constant stress.

As full details of the building were not available, an idealized case is modeled hereafter to examine the ability of the model to reproduce this feature of the frozen soil behavior. The main adapted parameters are listed in Table 4. The adopted mesh together with initial and boundary conditions, are shown in Fig. 22.

Movements are fully restricted at the bottom of the domain, whereas the soil can move in the vertical direction only at the lateral boundaries. An initial temperature of −10 °C is established throughout the boundary. The correspond initial unfrozen-water liquid saturation is S_l = 11.6% (Fig. 11.c). The bottom and lateral boundaries are considered impermeable. The soil is then loaded until 0.18 MPa, which is associated with the construction of the building. Afterward, the soil is thawed (i.e., stage relate to the operation of the building) by increasing the temperature of the soil (up to T = 0 °C) below the foundation only.

The stress paths of the soil subjected to these generalized stresses (i.e., involving temperature and net stresses changes) are shown

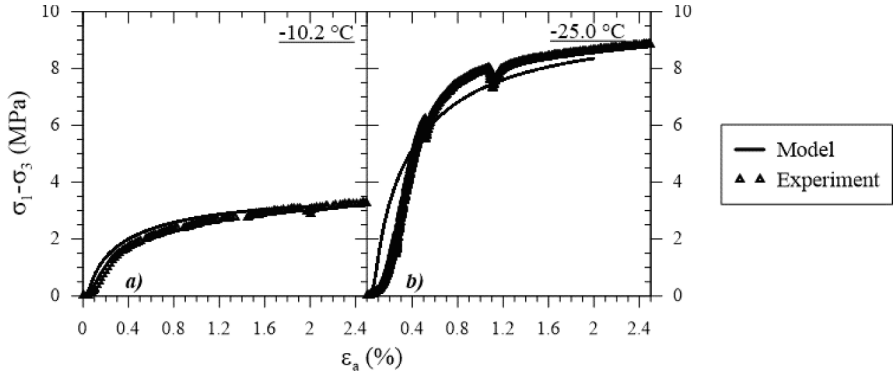

Fig. 20. Validation, experimental and modeling results involving unconfined compression tests at two temperatures: a) T = -10.2 °C and b) T = -25 °C.

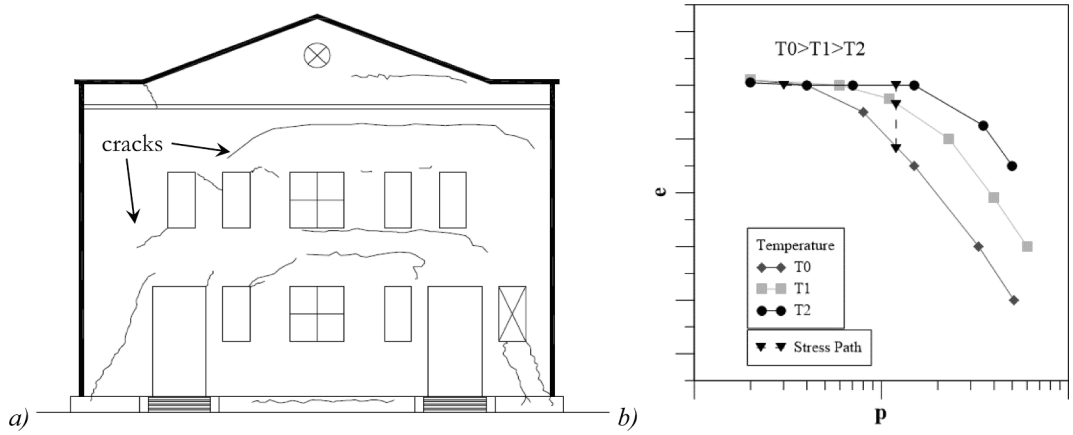

Fig. 21. a) Representation of the building subjected to thaw-collapse phenomenon Zhukov (1990); b) schematic representation of the generalized stress path in the e-p plane related to the loading (i.e., building construction) and thaw (i.e., building warming).

Table 4
Main constituive equations and material parameters.

Constitutive Model	Parameters*	Equation
Unfrozen-water retention curve	P = 0.90 [MPa]	(22)
	$\lambda = 0.45$	
Intrinsic permeability	$k_0 = 5.0 \times 10^{-15}$ [m^2]	(20)
	$n_0 = 0.40$	
Relative permeability	m = 3	(21)
Fourier's law	$\lambda_s = 5.00$ [W/(mC)]	(17)
	$\lambda_l = 0.58$ [W/(mC)]	
	$\lambda_i = 2.10$ [W/(mC)]	
Mechanical model	$\kappa = 0.001$	(6)
	$\lambda_0 = 0.028$	(6)
	p_o^*=0.07 [MPa]	(6)
	$p_c = 0.038$ [MPa]	(6)
	r = 0.21	(7)
	$\beta = 0.16$	(7)
	$\nu = 0.35$	(11)
	M = 0.07	(4)
	$\alpha = 3$	(4)
	n = 1	(4)
	$\gamma = 1/9$	(4)
	k = 0.41	(4)
		(8)

(*) The parameters not indicated in this table are set equal to the default values indicated in CODE_BRIGHT (2021).

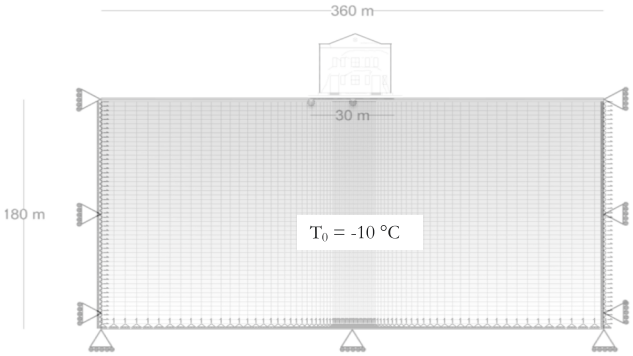

Fig. 22. Finite element mesh and boundary conditions assumed in the numerical simulations.

schematically in Fig. 23a) in the isotropic p-T (or p-s) plane and in Fig. 23b) in the void ratio net mean stress plane. Path A-B is related to the loading stage (i.e., building construction) under frozen conditions. The entire stress path moves along the elastic slope. Then, the soil warming starts, inducing the reduction of the cryonic suction with the corresponding soil thaw under constant stress conditions. During the thawing path, the LC yield curve is reached (i.e., point '★' Fig. 23a). Thawing beyond this point triggers plastic volumetric (compressive) deformations (with related enlargement of the yield surface) until reaching point D (Fig. 23b).

The contours of temperature and degree of saturation at the end of the analyzed period are shown in Fig. 24a and 24b, respectively. The maximum temperature is observed at the center of the building foundation-surface contact.

Fig. 25 depicts the corresponding contours of displacement when the temperature reaches 0 °C. The larger settlements are predicted at the center of the foundation leading, therefore, to differential settlements between the center and the edge of the foundation.

To illustrate in more detail the differential settlements, Fig. 26 shows the evolution of the vertical displacements at different temperatures at two positions, the edge, and the center, of the building foundation. The differential settlements predicted by the model are consistent with the failure patterns observed in the actual building.

6. Summary and conclusions

This work focuses on the mechanical behavior of natural frozen soils. We present the main results related to isotropic and shearing tests conducted on samples retrieved from Alaska and tested at Sandia National Laboratories. This data-set is unique, involving the mechanical behavior of natural frozen soils (information that is very scarce in the literature) and covering a wide range of temperatures (i.e., $-6\ °C < T < -26\ °C$), and confinements (i.e., $0 < \sigma_3 =< 54.6$ MPa). We also present an elasto-plastic model for frozen soils to analyze the mechanical tests conducted on the natural frozen soil samples. We implemented the elastoplastic model in a coupled thermo-hydro-mechanical finite element computer code adapted to deal with subzero temperatures. Finally, the proposed framework is applied to describe the thawing behavior of frozen soil under a building foundation.

From the experimental campaign on natural frozen samples, it was observed that the decrease of temperature (or increase in cryogenic suction) is associated with: an increase of apparent preconsolidation mean stress, a stiffening of the frozen soil (particularly for the virgin consolidation conditions), and an increment of soil strength. The soil also exhibits a smooth transition between elastic and plastic behaviors. Similar trends were observed in published studies based on reconstituted frozen soil samples. We also show that the adopted elasto-plastic model for frozen soils accounted for the main features of frozen soil behavior observed in the natural samples, namely: increase of stiffness, changes in preconsolidation pressure, and strength with the decrease of

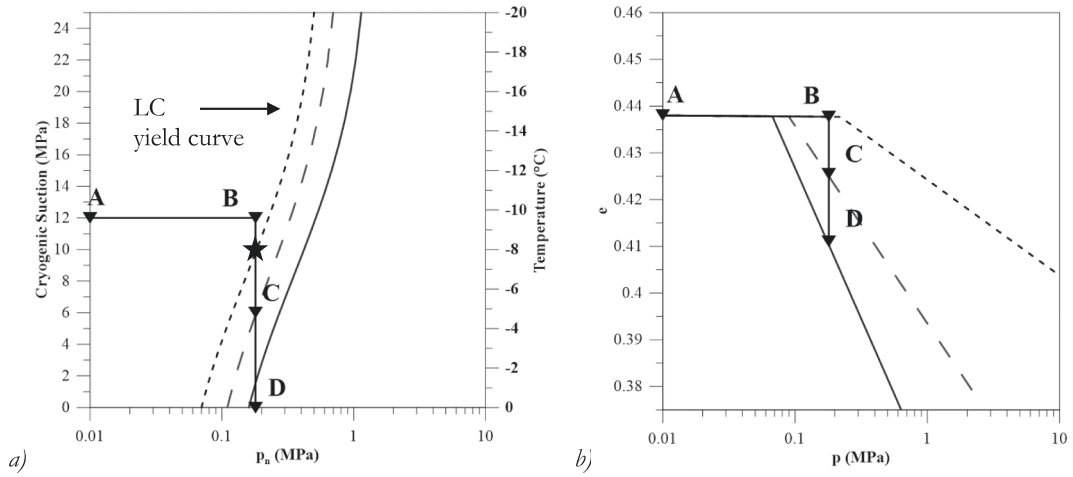

Fig. 23. Generalized stress path during loading and heating: a) e-log(p) and, b) p-s planes.

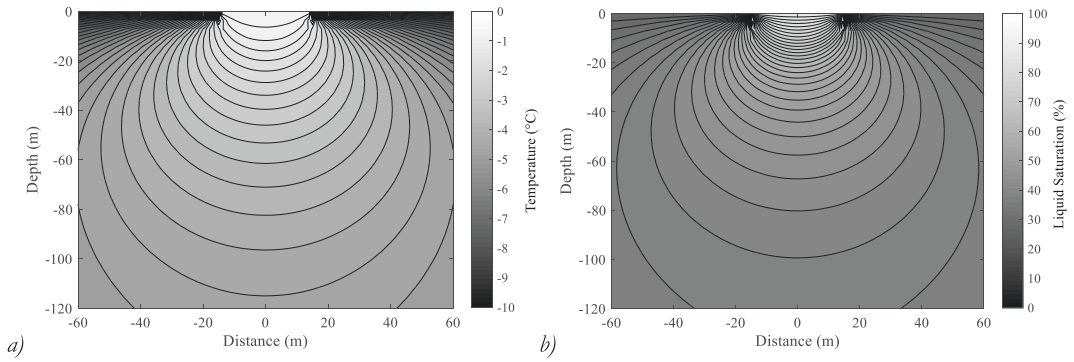

Fig. 24. Contours at steady state conditions: a) temperature, and b) unfrozen-water liquid saturation.

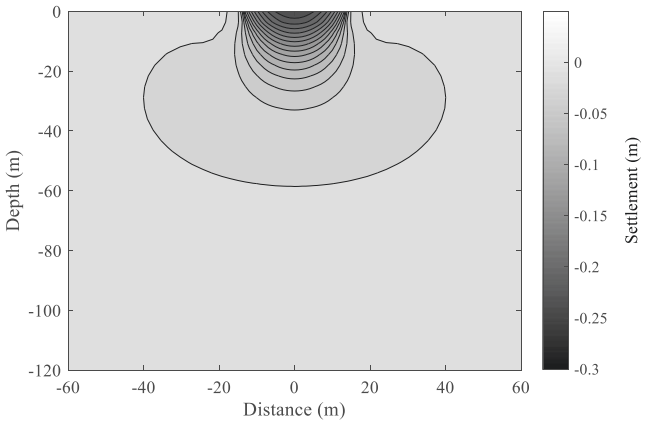

Fig. 25. Contours of settlement at the end of heating.

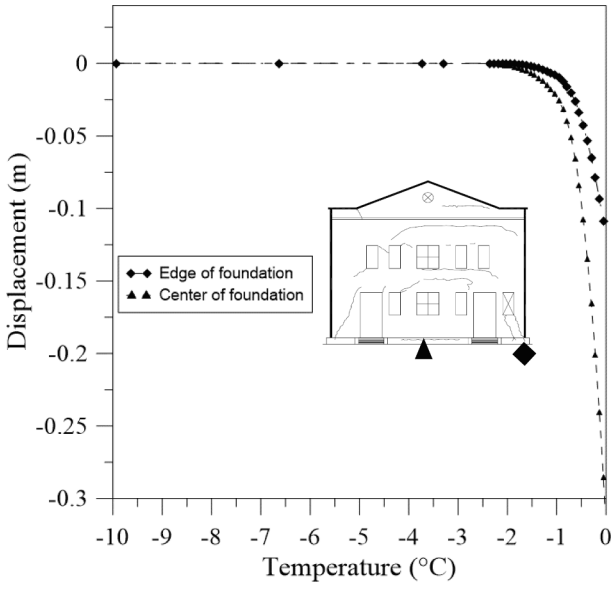

Fig. 26. Evolution of building settlements with the temperature at two positions, center and edge of the foundation.

temperature. The model was able to capture qualitatively well the soil volumetric behavior under different temperatures and confinements. The modeling (as a boundary value problem) of the warming of frozen soil under a building foundation indicates that the proposed framework can capture another key feature of frozen soil behavior relevant to geotechnical engineering in cold regions, as it is the volumetric collapse compression observed during frozen soil thawing which causes the largest disruption in surface structures.

CRediT authorship contribution statement

Ajay Shastri: Methodology, Software, Writing - original draft. **Marcelo Sánchez:** Conceptualization, Supervision, Funding acquisition, Writing - original draft. **Xuerui Gai:** Software. **Moo Y. Lee:** Methodology, Investigation, Funding acquisition. **Thomas Dewers:** Methodology, Funding acquisition, Writing - review & editing.

Declaration of Competing Interest

The authors declare the following financial interests/personal relationships, which may be considered as potential competing interests: Marcelo Sánchez reports financial support was provided by United States National Science Foundation.

Acknowledgments

We acknowledge the financial support from the United States National Science Foundation, award number: 2034204. Sandia National Laboratories is a multi-mission laboratory managed and operated by National Technology and Engineering Solutions of Sandia, LLC, a wholly owned subsidiary of Honeywell International Inc., for the US Department of Energy's National Nuclear Security Administration under contract DE-NA0003525. This paper describes objective technical results and analysis. Any subjective views or opinions that might be expressed in the paper do not necessarily represent the views of the US Department of Energy or the United States Government.

References

Alonso, E.E., Gens, A., Josa, A., 1990. A constitutive model for partially saturated soils. Géotechnique. 40 (3), 405–430. https://doi.org/10.1680/geot.1990.40.3.405.

Arenson, L.U., Johansen, M.M., Springman, S.M., 2004. Effects of volumetric ice content and strain rate on shear strength under triaxial conditions for frozen soil samples. Permafr Periglac Process. 15 (3), 261–271. https://doi.org/10.1002/(ISSN)1099-153010.1002/ppp.v15:310.1002/ppp.498.

Andersland, O.B., Ladanyi, B., 2003. Frozen Ground Engineering, 2nd Edition. John Wiley & Sons.

ASTM D4543. 2008. Standard Practices for Preparing Rock Core as Cylindrical Test Specimens and verifying Conformance to Dimensional and Shape Tolerances. ASTM 1–9.

Arenson, L.U., Springman, S.M., Sego, D.C., 2007. The rheology of frozen soils. Appl Rheol. 17 (1), 12147–1 - 12147–14 https://doi.org/10.1515/arh-2007-0003.

Arenson, Lukas U., Springman, Sarah M., 2005. Mathematical descriptions for the behaviour of ice-rich frozen soils at temperatures close to 0 °C. Artic Can Geotech J. 42 (2), 431–442. https://doi.org/10.1139/t04-109.

Beier, N.A., Sego, D.C., 2008. Cyclic freeze-thaw to enhance the stability of coal tailings. Cold Reg. Sci. Technol. 55 (3), 278–285. https://doi.org/10.1016/j.coldregions.2008.08.006.

Beskow, G., 1935. Tjalbildningen Och Tjallyftningen Med Sarskild Hansyn Till Vagar Och Jarnvagar.

Bekele, Y.W., Kyokawa, H., Kvarving, A.M., Kvamsdal, T., Nordal, S., 2017. Isogeometric analysis of THM coupled processes in ground freezing. Comput Geotech. 88, 129–145. https://doi.org/10.1016/j.compgeo.2017.02.020.

Clapeyron, B.P.É., 1834. Mémoire sur la puissance motrice de la chaleur. Journal de l'Ecole Polytech. 14, 153–190.

Clausius, R., 1850. Ueber die bewegende Kraft der Wärme und die Gesetze, welche sich daraus für die Wärmelehre selbst ableiten lassen. Ann Der Phys Und Chemie. 155 (4), 500–524. https://doi.org/10.1002/(ISSN)1521-388910.1002/andp.v155:410.1002/andp.18501550403.

Chen, Huie, Guo, Haotian, Yuan, Xiaoqing, Chen, Yating, Sun, Chao, 2020. Effect of temperature on the strength characteristics of unsaturated silty clay in seasonal Frozen Region. KSCE J Civ Eng. 24 (9), 2610–2620. https://doi.org/10.1007/s12205-020-1974-1.

CODE_BRIGHT Manual, 2021. Retrieve on 23rd March 2021. https://deca.upc.edu/en/projects/code_bright.

Ghoreishian Amiri, S.A., Grimstad, G., Kadivar, M., 2016. An elastic-viscoplastic model for saturated frozen soils. Eur. J. Environ. Civ. Eng. 1–17. https://doi.org/10.1080/19648189.2016.1271361.

Chuvilin, E.M., Bukhanov, B.A., Grebenkin, S.I., Doroshin, V.V., Iospa, A.V., 2018. Shear strength of frozen sand with dissociating pore methane hydrate: An experimental study. Cold Reg. Sci. Technol. 153, 101–105. https://doi.org/10.1016/j.coldregions.2018.04.013.

COUSSY, O, 2005. Poromechanics of freezing materials. J Mech Phys Solids. 53 (8), 1689–1718. https://doi.org/10.1016/j.jmps.2005.04.001.

Cui, Z.D., He, P.P., Yang, W.H., 2014. Mechanical properties of a silty clay subjected to freezing-thawing. Cold Reg. Sci. Technol. 98, 26–34. https://doi.org/10.1016/j.coldregions.10.009.

Czurda, K.A., Hohmann, M., 1997. Freezing effect on shear strength of clayey soils. Appl. Clay Sci. 12 (1-2), 165–187. https://doi.org/10.1016/S0169-1317(97)00005-7.

Da Re, G., Germaine, J.T., Ladd, C.C., 2003. Triaxial testing of frozen sand: equipment and example. Jnl. Cold Reg. Eng. 17, 90–118. https://doi.org/10.1061/(asce)0887-381x(2003)17:3(90).

De Guzman, E., Stafford, D., Alfaro, M.C., Doré, G., Arenson, L.U., 2018. Large-scale direct shear testing of compacted frozen soil under freezing and thawing conditions. Cold Reg. Sci. Technol. 151, 138–147. https://doi.org/10.1016/j.coldregions.2018.03.011.

Desai, C., 1989. Single surface yield and potential function plasticity. Comput. Geotech. 7 (4), 319–335.

Desai, C.S., Somasundaram, S., Frantziskonis, G., 1986. A hierarchical approach for constitutive modelling of geologic materials. Int. J. Numer. Anal. Methods Geomech. 10 (3), 225–257. https://doi.org/10.1002/(ISSN)1096-985310.1002/nag.v10:310.1002/nag.1610100302.

Esmaeili-Falak, M., Katebi, H., Javadi, A., 2018. Experimental study of the mechanical behavior of frozen soils – a case study of Tabriz subway. Periodica Polytechnica Civil Eng. 62 (1), 117–125. https://doi.org/10.3311/PPci.10960.

Esmaeili-Falak, M., Katebi, H., Javadi, A.A., 2020. Effect of freezing on stress-strain characteristics of granular and cohesive soils. J. Cold Reg. Eng. 34 (2), 05020001. https://doi.org/10.1061/(ASCE)CR.1943-5495.0000205.

Gai, X., Sánchez, M., 2017. A geomechanical model for gas hydrate-bearing sediments. Environ. Geotech. 4 (2), 143–156. https://doi.org/10.1680/jenge.15.00050.

Gai, X., Sánchez, M., 2019. An elastoplastic mechanical constitutive model for microbially mediated cemented soils. Acta Geotech. 14 (3), 709–726 https://doi.org/10.1007/s11440-018-0721-y.

GENS, A., 2010. Soil-environment interactions in geotechnical engineering. Geotechnique 60 (1), 3–74. https://doi.org/10.1680/geot.9.P.109.

Gens, A., Sánchez, M., Guimarães, L. Do N., Alonso, E.E., Lloret, A., Olivella, S., Villar, M. V., Huertas, F., 2009. A full-scale in situ heating test for high-level nuclear waste disposal: observations, analysis and interpretation. Géotechnique. 59 (4), 377–399.

Gilpin, R.R., 1980. A model for the prediction of ice lensing and frost heave in soils. Water Resource Res. 16 (5), 918–930. https://doi.org/10.1029/WR016i005p00918.

Goldman, E., 2002. Even in the high Arctic, nothing is permanent. Science 297 (5586), 1493–1494. https://doi.org/10.1126/science.297.5586.1493a.

Hashiguchi, K., 1989. Subloading surface model in unconventional plasticity. Int J Solids Struct. 25 (8), 917–945. https://doi.org/10.1016/0020-7683(89)90038-3.

Hashiguchi, K., Ueno, M., 1977. Elastoplastic constitutive laws of granular materials, constitutive equations of soils. 9th Int. Conf. Soil Mech. Found. Eng. Spec. Sess. 9, 73–82.

Harlan, R.L., 1973. Analysis of coupled heat-fluid transport in partially frozen soil. Water Resour. Res. 9 (5), 1314–1323.

Hohmann, Maria, 1997. Soil freezing - The concept of soil water potential. State of the art. Cold Reg. Sci. Technol. 25 (2), 101–110. https://doi.org/10.1016/S0165-232X(96)00019-5.

Jame, Yih-Wu, Norum, Donald I., 1980. Heat and mass transfer in a freezing unsaturated porous medium. Water Resour. Res. 16 (4), 811–819. https://doi.org/10.1029/WR016i004p00811.

Kim, A., 2011. Multi-Dimensional Frost Heave Modeling With Sp Porosity Growth Function. PhD Thesis. University of Alaska Fairbanks.

Kim, S.Y., Hong, W.T., Lee, J.S., 2018. Silt fraction effects of frozen soils on frozen water content, strength, and stiffness. Constr. Build. Mater. 183, 565–577. https://doi.org/10.1016/j.conbuildmat.2018.06.187.

Konrad, Jean-Marie, Morgenstern, Norbert R., 1980. A mechanistic theory of ice lens formation in fine-grained soils. Can. Geotech. J. 17 (4), 473–486. https://doi.org/10.1139/t80-056.

Konrad, J.M., Morgenstern, N.R., 1981. Segregation potential of a freezing soil. Can. Geotech. J. 18, 482–491. https://doi.org/10.1139/t81-059.

Konrad, J.-M., Morgenstern, N.R., 1984. Frost heave prediction of chilled pipelines buried in unfrozen soils. Can. Geotech. J. 21 (1), 100–115. https://doi.org/10.1139/t84-008.

Konrad, J.-M., Shen, M., 1996. 2-D frost action modeling using the segregation potential of soils. Cold Reg. Sci. Technol. 24 (3), 263–278. https://doi.org/10.1016/0165-232X(95)00028-A.

Lee, M.Y., Fossum, A., Costin, L.S., Bronowski, D., 2002. Frozen soil material testing and constitutive modeling. Sandia National Laboratories SAND Report, SAND2002-0524: 1–65.

Li, Ning, Chen, Feixiong, Su, Bo, Cheng, Guodong, 2002. Theoretical frame of the saturated freezing soil. Cold Reg. Sci. Technol. 35 (2), 73–80. https://doi.org/10.1016/S0165-232X(02)00029-0.

Li, Q., Ling, X., Sheng, D., 2016a. Elasto-plastic behaviour of frozen soil subjected to long-term low-level repeated loading, Part I: Experimental investigation. Cold Reg. Sci. Technol. 125, 138–151. https://doi.org/10.1016/j.coldregions.2015.11.015.

Li, Q., Ling, X., Sheng, D., 2016b. Elasto-plastic behaviour of frozen soil subjected to long-term low-level repeated loading, Part II: Constitutive modelling. Cold Reg. Sci. Technol. 122, 58–70. https://doi.org/10.1016/j.coldregions.2015.11.009.

Liu, Jiankun, Cui, Yinghui, Liu, Xin, Chang, Dan, 2020. Dynamic characteristics of warm frozen soil under direct shear test-comparison with dynamic triaxial test. Soil Dyn. Earthq. Eng. 133, 106114. https://doi.org/10.1016/j.soildyn.2020.106114.

Liu, Z., Liu, J., Li, X., Fang, J., 2019. Experimental study on the volume and strength change of an unsaturated silty clay upon freezing. Cold Reg. Sci. Technol. 157, 1–12. https://doi.org/10.1016/j.coldregions.2018.09.008.

Liu, Zhen, Yu, Xiong, 2011. Coupled thermo-hydro-mechanical model for porous materials under frost action: theory and implementation. Acta Geotech. 6 (2), 51–65. https://doi.org/10.1007/s11440-011-0135-6.

Ma, Wei, Chang, Xiaoxiao, 2002. Analyses of strength and deformation of an artificially frozen soil wall in underground engineering. Cold Reg. Sci. Technol. 34 (1), 11–17. https://doi.org/10.1016/S0165-232X(01)00042-8.

Michalowski, Radoslaw L., Zhu, Ming, 2006. Frost heave modelling using porosity rate function. Int. J. Numer. Anal. Methods Geomech. Int. J. Numer. Anal. Meth. Geomech. 30 (8), 703–722. https://doi.org/10.1002/(ISSN)1096-985310.1002/nag.v30:810.1002/nag.497.

Miller, R.D., Loch, J.P.G., Bresler, E., 1975. Transport of water and heat in a frozen permeameter. Soil Sci. Soc. Am. J. 39 (6), 1029–1036.

Multon, S., Sellier, A., Perrin, B., 2012. Numerical analysis of frost effects in porous media. Int. J. Num. Anal. Methods Geomech. 36, 438–458. https://doi.org/10.1002/nag.1014ï.

Newman, G.P., Wilson, G.W., 1997. Heat and mass transfer in unsaturated soils during freezing. Can. Geotech. J. 34 (1), 63–70. https://doi.org/10.1139/t96-085.

Nishimura, S., Gens, A., Olivella, S., Jardine, R.J., 2009. THM-coupled finite element analysis of frozen soil: formulation and application. Geotechnique 59 (3), 159–171 https://doi.org/10.1680/geot.2009.59.3.159.

Nixon, J.F., 1990. Effect of climatic warming on pile creep in permafrost. J. Cold Reg. Eng. 4 (1), 67–73. https://doi.org/10.1061/(ASCE)0887-381X(1990)4:1(67).

Olivella, S., Carrera, J., Gens, A., Alonso, E.E., 1994. Nonisothermal multiphase flow of brine and gas through saline media. Transp Porous Media. 15 (3), 271–293 https://doi.org/10.1007/BF00613282.

Olivella, S., Gens, A., Carrera, J., Alonso, E.E., 1996. Numerical formulation for a simulator (CODE_BRIGHT) for the coupled analysis of saline media. Eng. Computat. 13 (7), 87–112. https://doi.org/10.1108/02644409610151575.

O'Neill, Kevin, Miller, Robert D., 1985. Exploration of a rigid ice model of frost heave. Water Resour. Res. 21 (3), 281–296. https://doi.org/10.1029/WR021i003p00281.

Parameswaran, V.R., 1980. Deformation behaviour and strength of frozen sand. Can. Geotech. J. 17 (1), 74–88. https://doi.org/10.1139/t80-007.

Parameswaran, V.R., Jones, S.J., 1981. Triaxial testing of frozen sand. J. Glaciol. 27 (95), 147–155. https://doi.org/10.1017/S0022143000011308.

Parry, M., 2007. Climate Change 2007: Impacts, Adaptation and Vulnerability: Working Group II Contribution to the Fourth Assessment Report of the IPCC Intergovernmental.

Qi, Jilin, Hu, Wei, Ma, Wei, 2010. Experimental study of a pseudo-preconsolidation pressure in frozen soils. Cold Reg. Sci. Technol. 60 (3), 230–233. https://doi.org/10.1016/j.coldregions.2009.10.008.

Romero, Enrique, Sánchez, Marcelo, Gai, Xuerui, Barrera, Mauricio, Lloret, Antonio, 2019. Mechanical behavior of an unsaturated clayey silt: an experimental and constitutive modelling study. Can. Geotech. J. 56 (10), 1461–1474. https://doi.org/10.1139/cgj-2018-0117.

Sánchez, M., Gens, A., Villar, M.V., Olivella, S., 2016. Fully coupled thermo-hydro-mechanical double-porosity formulation for unsaturated soils. Int. J. Geomech. 16 (6), D4016015.

Sánchez, M., Shastri, A., Le, T.M.H., 2014. Coupled hydromechanical analysis of an underground compressed air energy storage facility in sandstone. Geotech. Lett. 4 (2), 157–164. https://doi.org/10.1680/geolett.13.00068.

Sayles, F.H., 1974. Triaxial constant strain rate tests and triaxial creep tests on frozen Ottawa sand. US Army Corps Eng. Cold Reg. Res. Eng. Lab. Tech. Rep. https://doi.org/10.1016/0148-9062(75)91294-2. [3].

Sinha, Nirmal K., 1989. Elasticity of natural types of polycrystalline ice. Cold Reg. Sci. Technol. 17 (2), 127–135. https://doi.org/10.1016/S0165-232X(89)80003-5.

Sheng, D., Axelsson, K., Knutsson, S., 1995. Frost heave due to ice lens formation in freezing soils 1. Theory and verification. Nordic Hydrolgy 26 (2), 125–146.

Sheng, D., Zhang, S., Niu, F., Cheng, G., 2014. A potential new frost heave mechanism in high-speed railway embankments. Geotechnique 64 (2), 144–154. https://doi.org/10.1680/geot.13.P.042.

Shoop, S., Affleck, R., Haehnel, R., Janoo, V., 2008. Mechanical behavior modeling of thaw-weakened soil. Cold Reg. Sci. Technol. 52 (1), 91–206. https://doi.org/10.1016/j.coldregions.2007.04.023.

Taber, Stephen, 1929. Frost heaving. J. Geol. 37 (5), 428–461. https://doi.org/10.1086/623637.

Tang, L., Cong, S., Geng, L., Ling, X., Gan, F., 2018. The effect of freeze-thaw cycling on the mechanical properties of expansive soils. Cold Reg. Sci. Technol. 145, 197–207. https://doi.org/10.1016/j.coldregions.2017.10.004.

Teng, Jidong, Yan, Han, Liang, Sihao, Zhang, Sheng, Sheng, Daichao, 2021. Generalising the Kozeny-Carman equation to frozen soils. J. Hydrol. 594, 125885. https://doi.org/10.1016/j.jhydrol.2020.125885.

Teymouri, M., Sánchez, M., Santamarina, J.C., 2020. A pseudo-kinetic model to simulate phase changes in hydrate bearing sediments. Mar. Pet. Geol. 120, 104519 https://doi.org/10.1016/j.marpetgeo.2020.104519.

Thomas, H.R., Cleall, P., Li, Y.-C., Harris, C., Kern-Luetschg, M., 2009. Modelling of cryogenic processes in permafrost and seasonally frozen soils. Geotechnique 59 (3), 173–184. https://doi.org/10.1680/geot.2009.59.3.173.

Tice, A.R., Anderson, D.M., Banin, A., 1973. The prediction of unfrozen water contents in frozen soils from liquid limit determinations. Symp. Frost Action Roads, Paris. 1, 329–344.

Tice, A.R., Black, P.B., Berg, R.L., 1989. Unfrozen water contents of undisturbed and remolded Alaskan silt. Cold Reg. Sci. Technol. 17 (2), 103–111. https://doi.org/10.1016/S0165-232X(89)80001-1.

van Genuchten, M.Th., 1980. A closed-form equation for predicting the hydraulic conductivity of unsaturated soils. Soil Sci. Soc. Am. J. 44 (5), 892–898. https://doi.org/10.2136/sssaj1980.03615995004400050002x.

Vitel, M., Rouabhi, A., Tijani, M., Guérin, F., 2016. Modeling heat and mass transfer during ground freezing subjected to high seepage velocities. Comput. Geotech. 73, 1–15. https://doi.org/10.1016/j.compgeo.2015.11.014.

Wang, Miao, Meng, Shangjiu, Sun, Yiqiang, Fu, Haiqing, 2018. Shear strength of frozen clay under freezing-thawing cycles using triaxial tests. Earthq Eng Eng Vib. 17 (4), 761–769. https://doi.org/10.1007/s11803-018-0474-5.

Watson, G., Rowley, R., Slusarchuk, W., 1973. Performance of a warm-oil pipeline buried in permafrost. Permafrost, North Am. Contrib. to Second Int. Conferance Permafr., Yakutsk, Siberia: NRC, Paper No 602.

Williams, P.J., 1964. Unfrozen water content of frozen soils and soil moisture suction. Geotechnique 14 (3), 231–246. https://doi.org/10.1680/geot.1964.14.3.231.

Xu, X., Li, Q., Lai, Y., Pang, W., Zhang, R., 2019. Effect of moisture content on mechanical and damage behavior of frozen loess under triaxial condition along with different confining pressures. Cold Reg. Sci. Technol. 157, 110–118. https://doi.org/10.1016/j.coldregions.2018.10.004.

Yamamoto, Yuko, Springman, Sarah M., 2014. Axial compression stress path tests on artificial frozen soil samples in a triaxial device at temperatures just below 0 °C. Can. Geotech. J. 51 (10), 1178–1195. https://doi.org/10.1139/cgj-2013-0257.

Yang, Yugui, Lai, Yuanming, Chang, Xiaoxiao, 2010. Laboratory and theoretical investigations on the deformation and strength behaviors of artificial frozen soil. Cold Reg. Sci. Technol. 64 (1), 39–45. https://doi.org/10.1016/j.coldregions.2010.07.003.

Zhang, Yao, Michalowski, Radoslaw L., 2015. Thermal-hydro-mechanical analysis of frost heave and thaw settlement. J. Geotech. Geoenvironmental. Eng. 141 (7), 04015027. https://doi.org/10.1061/(ASCE)GT.1943-5606.0001305.

Zhang, Z., Roman, L.T., Ma, W., Feng, W., Zhao, S., 2016a. The freeze-thaw cycles-time analogy method for forecasting long-term frozen soil strength. Measurement 92, 483–488. https://doi.org/10.1016/j.measurement.2016.06.044.

Zhang, Sheng, Sheng, Daichao, Zhao, Guotang, Niu, Fujun, He, Zuoyue, 2016b. Analysis of frost heave mechanisms in a high-speed railway embankment. Can. Geotech. J. 53 (3), 520–529.

Zhang, Hu, Zhang, Jianming, Zhang, Zhilong, Chen, Ji, You, Yanhui, 2016c. A consolidation model for estimating the settlement of warm permafrost. Comput. Geotech. 76, 43–50.

Zhang, Hu, Zhang, Jianming, Wang, Enliang, Zhang, Ze, Cao, Wei, Zhou, Panfeng, 2017. Thermal and settlement analyses under a riverbank over permafrost. Comput. Geotech. 91, 48–57 https://doi.org/10.1016/j.compgeo.2017.07.002.

Zhao, Futang, Chang, Lijun, Zhang, Wuyu, 2020. Experimental investigation of dynamic shear modulus and damping ratio of Qinghai-Tibet frozen silt under multi-stage cyclic loading. Cold Reg. Sci. Technol. 170, 102938. https://doi.org/10.1016/j.coldregions.2019.102938.

Zheng, B., Zhang, J., Qin, Y., 2010. Investigation for the deformation of embankment underlain by warm and ice-rich permafrost. Cold Reg. Sci. Technol. 60 (2), 161–168. https://doi.org/10.1016/j.coldregions.2009.08.012.

Zhou, Zhiwei, Ma, Wei, Zhang, Shujuan, Mu, Yanhu, Li, Guoyu, 2018. Effect of freeze-thaw cycles in mechanical behaviors of frozen loess. Cold. Reg. Sci. Technol. 146, 9–18.

Zhu, Fengpan, Chen, Lanyun, Yao, Yonghe, Zhao, Quanwei, Li, Junhu, 2020. Experimental study on direct shear mechanical characteristics of warm frozen silty clay. Ann. Chim. Sci. Des. Mater. 44 (1), 53–58.

Zhukov, V.F., 1990. Basic causes of deformation of buildings constructed on permafrost. Soil. Mech. Found Eng. 27, 174–178. https://doi.org/10.1007/BF02305651.